AD-A116 737 AIR FORCE INST OF TECH WRIGHT-PATTERSON AFB OH F/G 20/13
THERMAL RADIATION FROM HOT SURFACES MEASURED BY OPTICAL AND CAL--ETC(U)
1982 G T O'CONNOR
UNCLASSIFIED AFIT/NR-82-3T NL

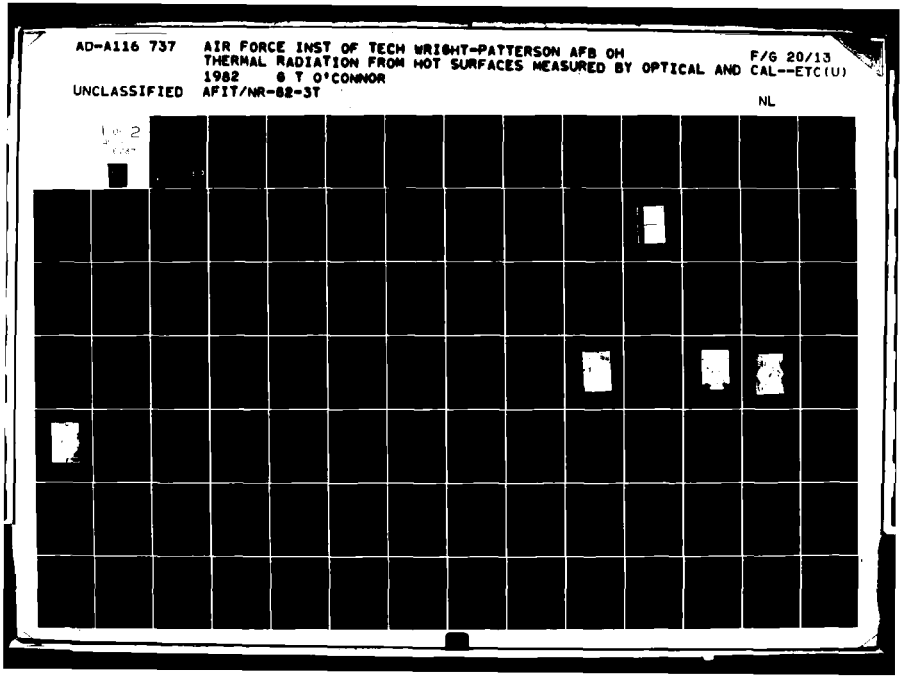

UNCLASS
SECURITY CLASSIFICATION OF THIS PAGE (When Data Entered)

(1)

REPORT DOCUMENTATION PAGE

READ INSTRUCTIONS BEFORE COMPLETING FORM

1. REPORT NUMBER: AFIT/NR 82-3T	2. GOVT ACCESSION NO.: AD-A116737
3. RECIPIENT'S CATALOG NUMBER:	
4. TITLE (and Subtitle): Thermal Radiation from Hot Surfaces Measured by Optical and Calorimetric Methods.	5. TYPE OF REPORT & PERIOD COVERED: THESIS/DISSERTATION/
	6. PERFORMING ORG. REPORT NUMBER:
7. AUTHOR(s): Gerald Thomas O'Connor	8. CONTRACT OR GRANT NUMBER(s):
9. PERFORMING ORGANIZATION NAME AND ADDRESS: AFIT STUDENT AT: University of Arizona	10. PROGRAM ELEMENT, PROJECT, TASK AREA & WORK UNIT NUMBERS:
11. CONTROLLING OFFICE NAME AND ADDRESS: AFIT/NR, WPAFB OH 45433	12. REPORT DATE: 1982
	13. NUMBER OF PAGES: 96
14. MONITORING AGENCY NAME & ADDRESS (if different from Controlling Office):	15. SECURITY CLASS. (of this report): UNCLASS
	15a. DECLASSIFICATION/DOWNGRADING SCHEDULE:

16. DISTRIBUTION STATEMENT (of this Report)

APPROVED FOR PUBLIC RELEASE; DISTRIBUTION UNLIMITED

17. DISTRIBUTION STATEMENT (of the abstract entered in Block 20, if different from Report)

LYNN E. WOLAVER
Dean for Research and
Professional Development
AIR FORCE INSTITUTE OF TECHNOLOGY (ATC)
WRIGHT-PATTERSON AFB, OH 45433

18. SUPPLEMENTARY NOTES

APPROVED FOR PUBLIC RELEASE: IAW AFR 190-17

22 JUN 1982

19. KEY WORDS (Continue on reverse side if necessary and identify by block number)

20. ABSTRACT (Continue on reverse side if necessary and identify by block number)

ATTACHED

82 07 07 055

DTIC ELECTE JUL 1 2 1982 S D E

DTIC FILE COPY

DD FORM 1 JAN 73 1473 EDITION OF 1 NOV 65 IS OBSOLETE

UNCLASS
SECURITY CLASSIFICATION OF THIS PAGE (When Data Entered)

82-3T

THERMAL RADIATION FROM HOT SURFACES MEASURED BY OPTICAL AND CALORIMETRIC METHODS

by

Gerald Thomas O'Connor

A Thesis Submitted to the Faculty of the

COMMITTEE ON OPTICAL SCIENCES (GRADUATE)

In Partial Fulfillment of the Requirements
For the Degree of

MASTER OF SCIENCE

In the Graduate College

THE UNIVERSITY OF ARIZONA

1 9 8 2

STATEMENT BY AUTHOR

This thesis has been submitted in partial fulfillment of requirements for an advanced degree at The University of Arizona and is deposited in the University Library to be made available to borrowers under the rules of the Library.

Brief quotations from this thesis are allowable without special permission, provided that accurate acknowledgment of source is made. Requests for permission for extended quotation from or reproduction of this manuscript in whole or in part may be granted by the head of the major department or the Dean of the Graduate College when in his judgment the proposed use of the material is in the interests of scholarship. In all other instance, however, permission must be obtained from the author.

SIGNED: Gerald T. O'Connor

APPROVAL BY THESIS DIRECTOR

This thesis has been approved on the date shown below:

B. O. Seraphin

B. O. SERAPHIN
Professor of Optical Sciences

December 16, 1981
Date

ACKNOWLEDGMENTS

I wish to thank all those involved in this study. Professor Seraphin especially deserves my gratitude for his expert care and guidance that insured I completed this project within the Air Force's stringent time constraints. He not only was patient and instructive, but still required that I perform up to his high standards. I would also like to thank Dr. Mike Jacobson, who gave invaluable aid in the laboratory. Also helpful were Paul Hillman, Liz Chain, Kyle Voss, and Peter Hey. I would like to thank Ms. Julio Quintana, who started this project. Drs. James Palmer and H. Angus Macleod both provided valuable inputs for the final draft of this thesis. My thanks also to Mrs. Norma Emptage who typed this in record time.

Finally, I would like to express my love and appreciation to my family, Winnie, Cari, and Tracy, who endured three stormy semesters.

TABLE OF CONTENTS

LIST OF ILLUSTRATIONS

LIST OF ILLUSTRATIONS--Continued

LIST OF TABLES

ABSTRACT

The radiative heat loss from a surface is determined by its total hemispherical emittance, which consequently plays an important role in aerospace and solar applications. This study compares emittances measured calorimetrically with values derived from near normal incidence spectral reflectance measurements. This optical derivation is based on a number of assumptions which limit the accuracy if not sufficiency fulfilled. These assumptions include sample specularity, a straybody character beyond the range of measurement, only small variations of emittance with temperature, and a perfectly smooth sample surface. The comparison of calorimetrically and optically derived emittance performed in this study not only quantifies the errors introduced by insufficient fulfillment of the assumptions but also identifies which assumption causes the dominant error. The calorimetric emissometer, constructed for this study and based on a heat flow sensor, was calibrated with aluminum and nickel thin films, resulting in good agreement with literature values. New data were obtained on "Black Molybdenum", a material promising for solar photothermal conversion produced by chemical vapor deposition. The study reports emittance values of a set of Black Molybdenum samples differing in their oxygen content, and thus varying in the values of their spectral selectivity.

CHAPTER 1

INTRODUCTION

The interaction of radiation with matter is described by two optical constants, the refractive index n, and the extinction coefficient k. The complementary process, the emission of thermal radiation from materials, is also determined by these two optical constants. Consequently, the energy transfer between surfaces by means of radiation can be expressed in terms of n and k.

The accuracy with which these optical constants can be extracted from the observables, absorptance, α, reflectance, ρ, transmittance, τ, and emittance, ε, depends on the spectral range, the optical properties of the material under consideration, and the characteristics of the radiating surface. Many studies have been made of various materials to determine these optical constants, but the results have been contradictory. For example, the Handbook of Chemistry and Physics in two different editions quotes values for platinum that "differ by a factor of 8 in refractive index and 2.8 in the extinction factor" (Siegel and Howell, 1972). New, significant applications of thermal radiation have been envisioned but require improved knowledge of these constants. It is important that improved methods of determining them be developed.

Modern technology is especially concerned with energy transfer by means of thermal radiation. Radiation is the primary method of heat

dissipation of reentering space vehicles and high speed aircraft. The space shuttle also has radiative panels for heat dissipation in space which are deployed when the cargo doors are opened. These panels must not only radiate heat away from the shuttle, but also not absorb solar radiation to the point that they add heat to the system. This requires the panels to have optical properties that maximize thermal emittance.

A more difficult task is faced in solar photothermal conversion. Here a solar collector must absorb solar radiation, and suppress re-radiation as it heats up. In high-temperature conversion systems, the task of suppressing the thermal reradiation is far more difficult than improving absorption. According to Carnot's principle, the higher the converter temperature, the more efficiently the incident solar radiation is converted to thermal energy. Thermodynamics dictates, however, that all materials reradiate increasingly more energy as their temperature rises. Finally an equilibrium temperature is reached, where the converter radiates away as much energy as it absorbs. Thus, the desired high temperatures for efficient energy conversion will be reached only if the thermal radiation is suppressed. Solar converters require new materials that will both absorb strongly in the solar spectrum and yet radiate very little in the thermal infrared.

The above two samples emphasize the importance of absorptance and emittance of radiating surfaces. Characterizing performance in either application requires the determination of the optical properties of the components. These properties, like all the observables, are functions of the optical constants, n, and k. As functions of common variables, these observables are interrelated. Current methods of

measuring these properties make use of these interrelationships, measuring one quantity to compute another.

This study addresses the problems arising in the determination of total hemispherical emittance. This property can be obtained by several means, one of which is a near-normal incidence spectral reflectance measurement. This measurement is used predominantly by the Solar Energy Group, Optical Sciences Center, University of Arizona, to provide the necessary spectral information required in the development of solar collector materials. However, it is questionable whether or not an accurate determination of the total hemispherical emittance is obtainable with only this data. To convert a near-normal incidence spectral reflectance measurement into a total hemispherical emittance value, certain assumptions must be made. These assumptions are:

(1) specular surface, *smooth* with respect to wavelength

(2) purity, in that there are *no* contaminants, oxide layers, etc.

(3) knowledge of n and k over the infrared region.

These conditions will rarely be fulfilled. As a result, the evaluation of total radiative loss, based on total hemispherical emittance derived from a near-normal incidence spectral reflectance, may only be approximate.

This study evaluates the total radiative loss as derived by a near-normal incidence spectral reflectance measurement and compares it to the value determined experimentally by a calorimetric method. The calorimetric method directly measures the total hemispherical emittance

and so provides the standard against which the optical derivation can be compared.

The test material for this study is a promising new material for high-temperature solar photothermal conversion developed by the Solar Energy Group at the Optical Sciences Center. It consists of a mixture of molybdenum and molybdenum dioxide which has been named "Black Molybdenum". This material has a high solar absorptance and low thermal emittance in a simple durable thin film deposited by Chemical Vapor Deposition (CVD), a process that may be expanded to large scale manufacturing. In order to evaluate fully the photothermal performance of this material, the total hemispherical emittance must be determined.

The three objectives of this thesis are:

(1) An evaluation of the total radiative heat loss as derived from a near normal incidence spectral reflectance measurement and as compared with a direct calorimetric measurement. The evaluation includes the theory behind the derivation of total hemispherical emittance from a reflectance measurement and a discussion of why this derivation may sometimes give only approximate results.

(2) A confirmation of the total hemispherical emittance of "Black Molybdenum", a promising solar converter material,

(3) A report on the construction of the Calorimetric Vacuum Emissometer (CVE) used in these measurements.

CHAPTER 2

SPECTRAL SELECTIVITY

A solar converter must have a high absorptance in the spectral region where solar radiation is strong and a low emittance in the thermal infrared to be spectrally selective. The purpose of this spectral selectivity is to elevate the equilibrium temperature of the converter to a point where the Carnot efficiency is high. If the converter cannot easily radiate infrared while absorbing solar radiation, the converter's temperature must rise until it starts radiating shorter wavelengths in sufficient quantity to reach thermal equilibrium. The diagram on the next page (Figure 2.1) illustrates spectral selectivity by a step function located at two microns. At wavelengths longer than two microns, the optimum converter has a zero emittance while at wavelengths shorter than two microns this same converter absorbs completely. A blackbody at the normal operating temperature of a solar converter will emit 95% of its radiation at wavelengths longer than two microns. If the converter's emittance approaches zero in this region, the converter will not radiate easily. Also, 95% of the energy in solar radiation is at wavelengths shorter than 2 microns, so the largest part of the available solar energy will be absorbed. This justifies the location of the step at 2 microns (Seraphin, 1981).

One way to compare solar converters is based on thermal efficiency η; one definition of which is

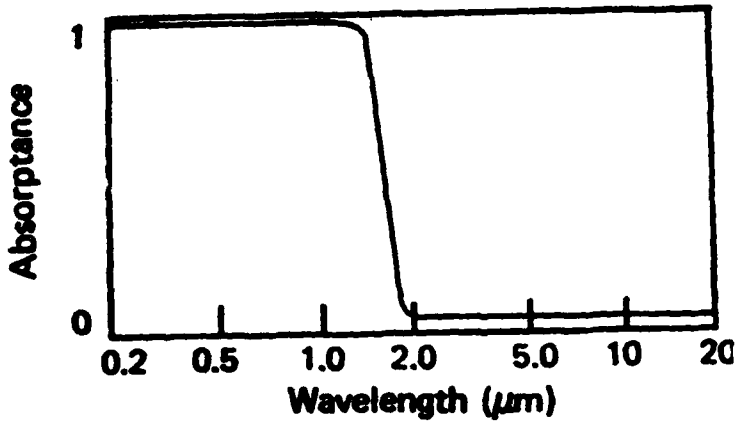

Figure 2.1. Optimum solar converter spectral porfile with high absorptance at wavelengths shorter than 2 microns and low emittance at wavelengths longer than 2 microns.

$$\eta = \frac{Q_{abs} - Q_{rerad} - Q_{conv} - Q_{cond}}{Q_{incident}} \qquad (2.1)$$

where Q_{abs} is the heat absorbed, Q_{rerad} the energy reradiated, and Q_{conv} and Q_{cond} the heat losses due to convection and conduction. $Q_{incident}$ is the total energy incident on the converter. This thesis is concerned with the evaluation of the optical properties of surfaces, in particular the absorptance and emittance. The reduction of convective and conductive losses are primarily engineering problems and so are not pertinent to this thesis; they will be ignored in further discussion. Thus, the purely radiative thermal efficiency is

$$\eta = \alpha_s - \frac{1}{\phi\tau X}\left[F(\varepsilon_{t_1}, \varepsilon_{t_2})(T_1^4 - T_2^4)\right] \qquad (2.2)$$

where

α_s = Solar absorptance

ε_{t_1} = Thermal emittance of absorber surface

ε_{t_2} = Thermal emittance of environment surrounding absorber surface

$F(\varepsilon_{t_1}, \varepsilon_{t_2})$ = Function of ε_{t_1} and ε_{t_2} determined by receiver geometry and orientation

σ = Stefan-Boltzmann constant (5.6×10^{-8} W m^{-2} k^{-4})

τ = Transmittance through system optics

ϕ = Insolation (direct for most concentrating systems)

T_1 = Surface temperature of the absorber surface

T_2 = Temperature of environment surrounding receiver

The concerntration factor X is given by

$$X = E \rho Ac/Ar \tag{2.3}$$

where

Ac = Effective aperture area of concentrator mirror or lens

Ar = Reradiating area of external reciever

E = (1-e) where e is the fraction of energy lost due to mirror surface imperfections and sun tracking errors

ρ = Specular reflectance of mirror surface within the maximum useful cone angle

As a final similification, η reduces to

$$\eta = \alpha_s - \beta\varepsilon_t \tag{2.4}$$

where

$$\beta = \frac{\sigma [T_1^4 - T_2^4]}{\phi \tau E \rho Ac/Ar} \tag{2.5}$$

Thermal efficiency has now been defined in terms of spectral selectivity and in parameters that depend on the characteristics of the system. For different applications, the importance of maximizing α_s as opposed to minimizing the thermal emittance ε_t varies. A small β implies that reradiation losses are minimal and α_s should be maximized. A large β implies that good spectral selectivity is critical. The figure on the next page (Figure 2.2) shows the benefits of spectral selectivity for systems of different concentration factors, X operating at different temperatures. Spectrally selective converters, which generally sacrifice a small amount of absorptance to obtain the low

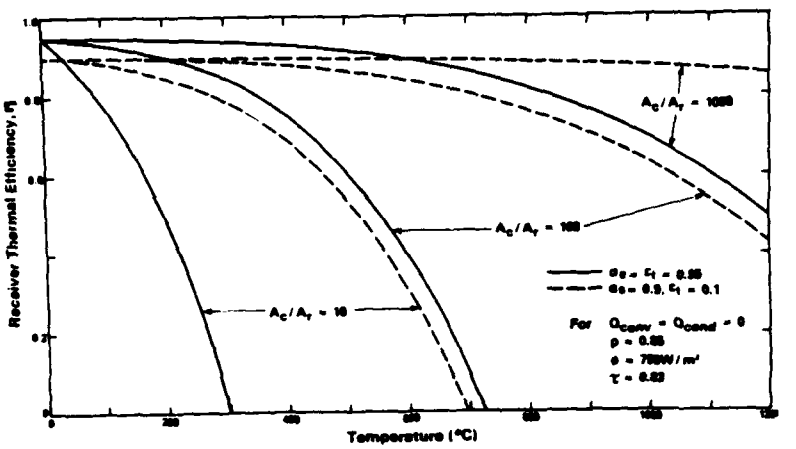

Figure 2.2. Receiver thermal efficiency, η, as a function of temperature, and showing the advantage of spectrally selectivesystems for different concentration factors (Seraphin, 1981).

emittance, drastically outperform non-selective systems at the lower temperatures and intermediate concentration factors (Seraphin, 1981).

There are several physical mechanisms by which spectral selectivity can be generated. Some of these mechanisms are not fully understood. This is the result of the difficulty in separating these mechanisms for individual study and the lack of attempts to do so. The effort must be made, however, so that a systematic design of an optimum converter can be accomplished. Even then, it will probably take the tandem action of several mechanisms to produce sufficient selectivity.

Metals generally have the high infrared reflectance required for low thermal emittance. However, their solar absorptance is inadequate for good selectivity. The emittance and absorptance of metals is a function of the metal's free and bound electrons, respectively. Since the transition metals and rare earths have a large variety in free and bound states, they deserve further investigation. In fact, this is one reason molybdenum was studied by the Optical Sciences Center.

One way to boost the solar absorptance of metals is to overcoat them with a thin film of high absorptance in the visible and near infrared but transparent in the thermal infrared region. This configuration is called a dark mirror. Semiconductors are frequently chosen for this task, since interband transitions of electrons provide the necessary absorptance while the material is transparent to the infrared. When the semiconductor absorbs solar photons, it heats the lower metallic layer, which has the necessary low thermal emittance to retain the heat. The semiconductor must be specifically chosen for the

spectral location of the absorption edge. This bilayer converter must also be made antireflective by an interference coating or surface texture to reduce front surface reflection losses.

Another bilayer configuration is the heat mirror. Here, a selective reflector covers the absorber. The absorber can now have a high absorptance over a range larger than just the solar sepctrum, since the reflector is responsible for the selectivity. The reflector must have a high transmittance in the solar spectrum but have a high infrared reflectance. This configuration traps the heat in the absorber, while the selective reflector on top suppresses the thermal reradiation loss. This method is not used as often as the dark mirror or other methods.

Multilayer interference coatings themselves can be used to provide the necessary solar absorptance. Very high selectivity has been achieved in this manner but the "tuned cavity" character of an interference filter makes it sensitive to degradation by slight changes of several parameters. Long-term deterioration from high temperature operation, sensitivity of performance to angle of incidence, and cost and complexity of manufacture discourage the use of interference filters.

Surface texture can greatly assist absorption and interference. There are three basic effects, depending roughly on the wavelength of light. Grooves and pores can increase the effective absorbing area by multiple reflections. These surfaces distinguish between the wavelengths, absorbing in the solar region but appearing smooth and reflective in the infrared. Manipulating the index of refraction by introducing a sufficient density of voids defines the second category.

Resonant scattering is the third textural effect, where very small particles embedded in a host matrix can, depending on the optical properties of the particles and the matrix, approximate the desired spectral profile by quantum effects.

The Solar Energy Group in the Optical Sciences Center, with which this work was completed, became interested in molybdenum thin films for several reasons. Like most metals, molybdenum has a high infrared reflectance. It has a high melting point, which means it does not agglomerate when used at solar converter operating temperatures. It is refractory, which means it is able to be heated to a very high degree without changing chemically or becoming soft. Molybdenum can be prepared in the thin film form, bypassing the expense of using large quantities of molybdenum. Finally, molybdenum has a lower visible reflectance, i.e., higher solar absorptance, than most metals, thus making it a good candidate for high spectral selectivity.

The CVD process was used to keep the eventual cost of manufacture down. At first the CVD molybdenum thin films did not approach the reflectance of bulk or sputtered molybdenum. It was then discovered that a high temperature anneal (800 C) for thirty minutes resulted in a thin film of relatively pure molybdenum. By varying the CVD process parameters and the annealing time, molybdenum thin films were finally produced that had a reflectance even higher than bulk molybdenum. These films, although containing traces of oxygen and carbon, were dubbed "Super Moly" because of their high reflectance.

The drastic change of the optical properties of molybdenum caused by annealing was an area of intense interest. It was found that during the annealing process, the infrared reflectance improved faster than the solar absorptance diminished. Stated another way, this meant the solar absorptance to infrared emittance ratio could be controlled and maximized. These thin films of partially annealed molybdenum were titled "Black Molybdenum", because of a black or smoky appearance to the eye.

"Black Molybdenum" is a mixture of individual metallic clusters embedded in a host matrix of the dielectric molybdenum dioxide. Figure 2.3 is a photograph taken with a scanning electron microscope of the surface of Black Molybdenum. This composite material can be adjusted over a range of absorptance-emittance values by varying the CVD process parameters and the annealing time and temperature. The advantage of "Black Molybdenum" over "Super Moly" in thin film stacks is simplicity. Although "Super Moly" has a lower infrared emittance, it must be overcoated with a selective absorber to be used in the dark mirror configuration. Both forms of molybdenum must then be overcoated with a passivator to prevent long-term degradation. The "Black Molybdenum" only needs one additional layer, as opposed to the two needed by "Super Moly". This simplicity lowers cost and improves durability, as the more layers in a stock, the higher the probability of deterioration. It was also found that the absorptance of "Black Molybdenum" could be further enhanced by chosing the thickness of the passivator layer to act as a single interference layer.

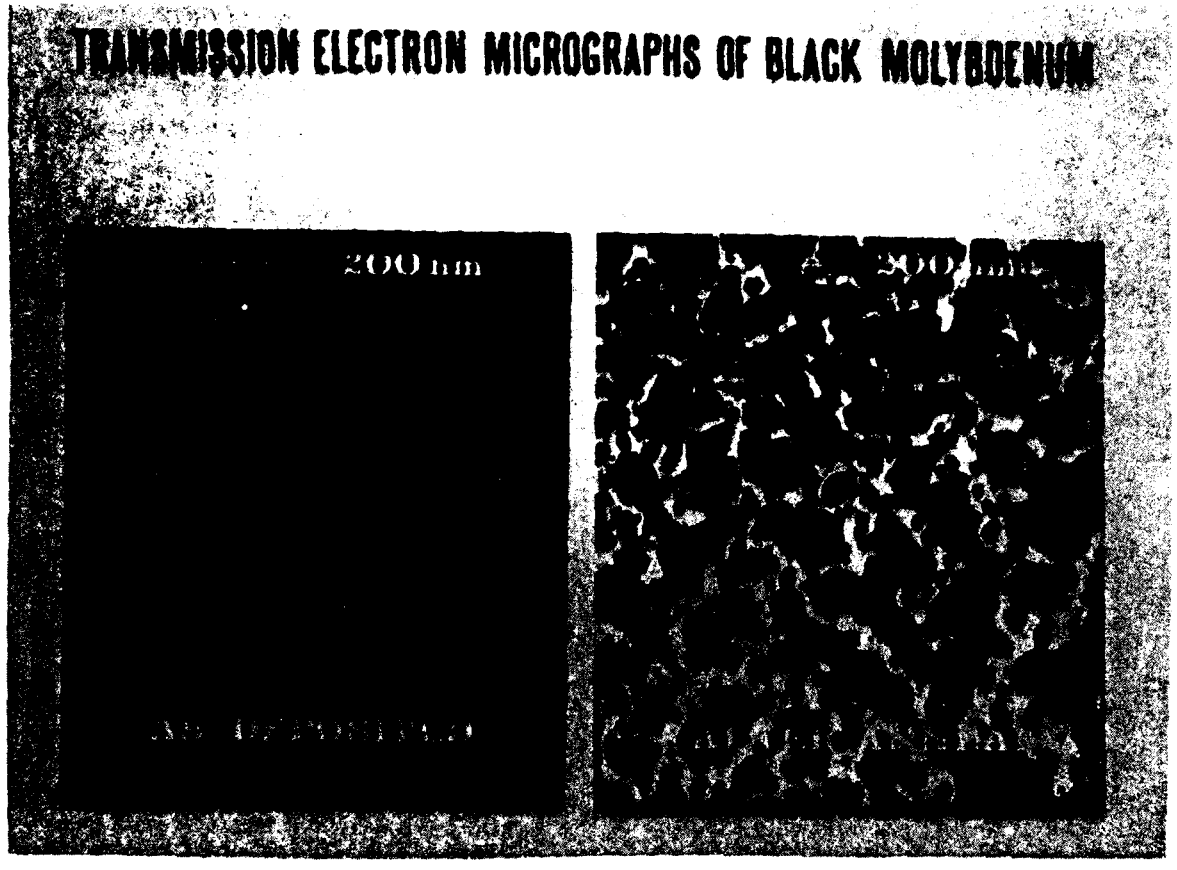

Figure 2.3. Transmission electron micrographs of Black Molybdenum.

The performance of these samples was determined by spectral reflectance measurements. Spectral reflectance measurements provided the necessary spectral information to compare the test material with the step function profile described in this chapter. The spectral reflectance, however, is only indirectly correlated with the total radiative loss of the sample; the total hemispherical emittance is the needed quantity. Although relationships do exist between reflectance and emittance, these relationships are not always valid. The actual thermal emittance of a complex surface, such as these molybdenum thin films, could be quite different than the reflectance measurements suggest. This thesis now provides a direct method for emittance measurement unhampered by surface structure and other assumptions or approximations. The next chapter wi . discuss the optical observables, emittance, absorptance, and reflectance, and relationships between them for the purpose of showing the potential errors caused by indirect measurement methods.

CHAPTER 3

OPTICAL PROPERTIES AND THEIR INTERRELATIONSHIPS

The three optical quantities of absorptance, emittance, and reflectance will be discussed in this chapter. They are observable characteristics of the optical constants, n and k. Since they are all functions of the same variables, it is reasonable to expect relationships among them. This chapter will define these three observables and show some relationships among them. Since most quoted values for emittance and absorptance are not the result of direct measurement, a strong understanding of the interrelationships of absorptance, emittance, and reflectance is necessary to evaluate the validity of the measurement method. This evaluation will be described in the next chapter.

Properties of Blackbodies

Emittance is measured against a fictional standard, called a blackbody. A blackbody is a material whose surface is a perfect absorber of all incident radiation at all wavelengths. Although some materials can approach blackbody performance in some spectral regions, no real blackbody exists. Consider a blackbody in a cavity surrounded by a material whose surface is also a blackbody and is otherwise perfectly insulated from the rest of the world. The enclosed blackbody absorbs all the radiation from the walls and the walls absorb all the radiation from the enclosed blackbody. The Second Law of Thermodynamics requires

that the net flow of energy must be from the warmer body to the cooler one. Therefore, the blackbody and the surrounding material must come to thermal equilibrium. Since, by definition, a blackbody absorbs all incident radiation, each blackbody in thermal equilibrium must emit as much as it absorbs at each wavelength. Therefore, blackbodies are said to be perfect emitters, and emittance of non-blackbodies is measured as the fraction of radiant energy that would be emitted by a blackbody under similar conditions.

The enclosed blackbody can also show that blackbodies are perfect emitters in each direction and at every wavelength. It can also be shown that the enclosed radiation field is isotropic. More importantly, since the absorbed and emitted radiant energy are equal only when the blackbody is at thermal equilibrium, without further conditions, it is therefore apparent that blackbody radiation is only a function of temperature.

The spectral qualities of a blackbody are described by several formulae. The wavelength dependence is given by Planck's spectral distribution, according to which the spectral exitance of a blackbody energy per unit area per unit wavelength is

$$M_{e\lambda} = \frac{2\pi hc^2}{\lambda^5}\left[\frac{1}{e^{hc/\lambda KT}-1}\right] . \qquad (3.1)$$

The derivation of this equation is associated with the beginnings of quantum mechanics. The peak of this curve, the primary wavelength associated with any specific temperature, is given by Wien's Displacement Law,

$$\lambda T = 2898 \ \mu m \ K \tag{3.2}$$

If Planck's distribution is integrated over all wavelengths, the temperature dependence of the total radiant power per area can be calculated. This is the Stefan-Boltzmann Law, which for a blackbody can be written as

$$M = \sigma T^4 \tag{3.3a}$$

where M is the total exitance and σ is the Stefan-Boltzmann constant. Real materials, unlike blackbodies, are not perfect radiators at all frequencies and in all directions. The amount of radiation they emit is always less. This is where the definition of emittance appears. The ratio of the radiated power of a real surface to the power radiated from the same area of a blackbody at the same temperature is called emittance. The Stefan-Boltzmann equation can be modified for use with real surfaces by including this factor:

$$M = \varepsilon \sigma T^4 \tag{3.3b}$$

Emittance and Absorptance

Emissivity is the material's intrinsic ability to radiate. Emittance, on the other hand, is the measured quantity of a sample, which can vary from an emissivity for several reasons, such as surface roughness and oxide layers. Emittance is dependent on body temperature, wavelength, and angle at which the energy is being emitted. $\varepsilon_\lambda'(\lambda,\theta,\phi,T)$ is a directional spectral emittance, where the direction is specified by θ and ϕ, the elevation and azimuth angles, the wavelength by λ, and the temperature by T.[1] Emittance can also be averaged over wavelength, direction, or both. Thus one can also speak of directional total emittance ε' hemispherical spectral emittance, ε_λ, or total hemispherical emittance ε. It is this quantity, total hemispherical emittance, that is used in the Stefan-Boltzmann equation for real surfaces.

In the same manner, absorptivity is the ideal property of a real material; absorptance is the measured quantity. Absorptance is slightly more complicated than emittance, however, because in addition to the material, the incident radiation must also be considered, like

---

1. To specify precisely the optical constants of real materials, a convention must be used, because of the large number of independent variables involved. The notation used in this paper is adopted from Siegel and Howell's book, Thermal Radiation Heat Transfer. Functional notation is used to show upon which variables a quantity depends, e.g., $\varepsilon_\lambda'(\lambda,\theta,\phi,T)$ shows a dependence on the four variables noted. Since the radiative properties depend on direction, primed quantities represent directional quantitiies while unprimed quantities represent hemispherical qunatities. The subscripts show a spectral dependence while the absence of a subscript shows that the wavelength dependence has been eliminated. The letter L will be used for radiance and will use the same superscripts, subscripts, and functional form as described above. In addition, radiance may also have the subscripts i, r, and b refering to incident, reflected, or blackbody radiation, respectively. An integration over 2π implies an intregration over the hemisphere.

emittance, absorptance is a function of wavelength, incident angle, and temperature, and so shares the same modifiers, e.g., directional spectral total hemispherical, etc. Its functional dependence is also shown in the same way, so that $\varepsilon_\lambda'(\lambda,\theta,\phi,T)$ is a directional spectral absorptance.

Absorptance and emittance can be even more closely tied together for real materials, if proper care is taken, Kirchhoff's Law is concerned with the relationship between emittance and absorptance for real materials. It is frequently and incorrectly applied by stating absorptance and emittance are equal when the material is at thermal equilibrium with its surroundings. There are times that this is true but only under additional conditions.

Kirchhoff's Law

Kirchhoff's Law can be applied in several cases. The most general case of Kirchhoff's Law is that at a given temperature, a material's directional spectral emittance and its directional spectral absorptance are equal:

$$\varepsilon_\lambda'(\lambda,\theta,\phi,T) = \alpha_\lambda'(\lambda,\theta,\phi,T) \tag{3.4}$$

This is a fixed property of all materials and holds without restriction. Kirchhoff's Law also applies to the directional total case. Directional total absorptance can be defined as:

$$\alpha'(\theta,\phi,T) = \frac{\int_0^\infty \alpha_\lambda'(\lambda,\beta,\theta,\phi)\ L'_{\lambda,i}(\lambda,\theta,\phi)\delta\lambda}{\int_0^\infty i'_{\lambda,i}(\lambda,\theta,\phi)\delta\lambda} \tag{3.5}$$

where $i'_{\lambda,i}(\lambda,\theta,\phi)$ is the incident spectral radiance. By use of Kirchhoff's Law, this can be written as:

$$\alpha'(\theta,\phi,T) = \frac{\int_0^\infty \varepsilon_\lambda'(\lambda,\theta,\phi)\ L'_{\lambda,i}(\lambda,\theta,\phi)\delta\lambda}{\int_0^\infty L'_{\lambda,i}(\lambda,\theta,\phi)\delta\lambda} \tag{3.6}$$

If the incident radiation has a spectral distribution proportional to that of a blackbody at T, then

$$L'_{\lambda,i}(\lambda,\theta,\phi) = c(\theta,\phi)\ L_{\lambda,b}(\lambda,T) \tag{3.7}$$

where $c(\theta,\phi)$ is an arbitrary function, and

$$\alpha'(\theta,\phi,T) = \frac{\int_0^\infty \varepsilon_\lambda'(\lambda,\theta,\phi)\ L_{\lambda,b}(\lambda,T)\delta\lambda}{\int_0^\infty L_{\lambda,b}(\lambda,T)\ \lambda = \sigma T^4/\pi} \tag{3.8}$$

But, this is the definition of directional total emittance. Therefore, if the incident radiation is proportional to that of a blackbody, then the directional total absorptance equals the directional total emittance.

There is another case where $\alpha'(\theta,\phi,T) = \varepsilon'(\theta,\phi,T)$ is valid. Directional spectral emittance can be defined as

$$\varepsilon_\lambda'(\lambda,\theta,\phi,T) = \frac{L'_\lambda(\lambda,\theta,\phi,T)}{L_{\lambda,b}(\lambda,\theta,\phi,T)} \tag{3.9}$$

If the directional emitted radiation from the surface is proportional to a blackbody, then,

$$L'_\lambda(\lambda,\theta,\phi,T) = c(\theta,\phi)\ L_{\lambda,b}\ (\lambda,T) \tag{3.10}$$

where again $c(\theta,\phi)$ is an arbitrary function. A surface with this kind of behavior is called a directional gray surface. Putting Eq. 3.10 into the definition of directional spectral emittance, Eq. 3.9,

$$\varepsilon_\lambda'(\lambda,\beta,\theta,T) = c(\theta,\phi) \tag{3.11}$$

The directional spectral emittance is independent of wavelength. This means that the directional total emittance, as defined in the right portion of Eq. 3.8 is also independent of wavelength, i.e., $\varepsilon_\lambda' = \varepsilon'$. From Kirchhoff's Law, $\varepsilon_\lambda' = \alpha_\lambda'$, and from Eq. 3.8 above, $\alpha' = \varepsilon_\lambda'$. Therefore, all four quantities are equal, and especially $\alpha' = \varepsilon'$.

There are also two applications of Kirchhoff's Law for hemispherical spectral absorptance and emittance. Hemispherical spectral absorptance is defined as

$$\alpha_\lambda = \frac{\int_{2\pi} \alpha_\lambda'(\lambda,\theta,\phi,T)\ L_{\lambda,i}(\lambda,\theta,\phi)\ \cos\theta\ \delta\omega}{\int_{2\pi} L'_{\lambda,i}(\lambda,\theta,\phi)\cos\theta\ \delta\omega} \tag{3.12}$$

where the directional spectral absorptance is integrated over a hemisphere. Using Kirchhoff's Law, this can be rewritten as

$$\alpha_\lambda = \frac{\int_{2\pi} \varepsilon_\lambda'(\lambda,\theta,\phi,T)\, L_{\lambda,i}(\lambda,\theta,\phi)\, \cos\theta\, \delta\omega}{\int L'_{\lambda,i}(\lambda,\theta,\phi)\, \cos\theta\, \delta\omega} \tag{3.13}$$

When α_λ' and ε_λ' are functions of λ,θ,ϕ, and T, $\alpha_\lambda = \varepsilon_\lambda$ only if the incident spectral radiance is uniform over all directions, i.e., independent of θ and ϕ. This allows the last equation to be rewritten as

$$\alpha_\lambda = \frac{\int_{2\pi} \varepsilon_\lambda'(\lambda,\theta,\phi,T)\, \cos\theta\, \delta\omega}{\int_{2\pi} \cos\theta\, \delta\omega} \tag{3.14}$$

The denominator is equal to π, which turns this equation into the definition of hemispherical spectral emittance:

$$\varepsilon_\lambda = \frac{1}{\pi} \int_{2\pi} \varepsilon_\lambda'(\lambda,\theta,\phi,T)\, \cos\beta\, \delta\omega \quad . \tag{3.15}$$

Therefore, with uniform incident radiance, total hemispherical absorptance equals spectral hemispherical emittance.

The second hemispherical spectral case is derived when the directional spectral quantitites are independent of angle.

$$\begin{aligned} \varepsilon_\lambda'(\lambda,\theta,\phi,T) &= \varepsilon_\lambda'(\lambda,T) \\ \alpha_\lambda'(\lambda,\theta,\phi,T) &= \alpha_\lambda'(\lambda,T) \end{aligned} \tag{3.16}$$

This kind of surface is a diffuse spectral surface, i.e., $\varepsilon_\lambda = \alpha_\lambda$.

Kirchhoff's Law applied to the hemispherical total case is understandably complicated. Hemispherical total quantities are averaged by integrating over both wavelength and angle. Although the order of integration is not important the constraints required to apply Kirchhoff's Law are. Since each integration has two possible requirements to satisfy before applying Kirchhoff's Law, the double integration has four possible combinations under which Kirchhoff's Law applies. The simplest case is the diffuse-gray case, where the directional quantities doe not depend on direction and the spectral quantitites doe not depend on wavelength. Thus,

$$\varepsilon = \varepsilon_\lambda' = \alpha_\lambda' = \alpha.$$

The above theoretical discussion has omitted one important practical datum. Neither absorptance nor emittance is as easy to measure as is reflectance. However, for opaque bodies, incident radiation is either reflected or absorbed, and with the above relationships between absorptance and emittance, all three quantities can be related. The following discussion will cover the definitions of the various reflectance quantities, and then derive the relationships between the three observables. This will permit us in Chapter 4 to evaluate the use of those relationships to obtain emittance values from reflectance measurements.

Reflectance

As emittance and absorptance, reflectance is the measured quantity and is a function of the material's reflectivity and surface conditions. The primary reflectance is bidirectional spectral reflectance, $\rho_\lambda''(\lambda,\theta_r,\phi_r,\theta,\phi,T)$ where some of the radiation incident at angle (θ,ϕ) will be reflected in the (θ_r,ϕ_r) direction.[2] To find the magnitude of all the reflected radiation, it will be necessary to sum over all possible angles (θ_r,ϕ_r) a hemisphere for a flat surface. Bidirectional spectral reflectance is the ratio of the directional spectral radiance reflected at a specified angle to the spectral radiance incident at another specified angle:

$$\rho_\lambda''(\lambda,\theta_r,\phi_r,\theta,\phi,T) = \frac{L_\lambda'',r(\lambda,\theta_r,\phi_r,\theta,\phi,T)}{L_{\lambda,i}(\lambda,\theta,\phi)\cos\theta} \qquad (3.18)$$

The $\cos\theta$ is required to correct for the amount of energy reflected by the projected area of the surface. For a diffuse reflection, the incident energy from (θ,ϕ) will be distributed evenly around all reflected angles $(\theta_r\phi_r)$. It is also generally true that bidirectional spectral reflectance is symmetric with respect to incident and reflected angles, i.e.,

---

2. Reflectivity is again more complicated than either emissivity or absorptivity, because the direction of the reflected energy must also be specified in addition to the incident direction. The notation already described will be continued, with two additions. A double prime will be used when the reflected direction as well as the incident direction are specified, and the functional notation will also show up to two sets of angles with subscripts to specify reflected variables. Angles not shown have been integrated over the hemisphere.

$$\rho_\lambda''(\lambda,\theta_r,\phi_r,\theta,\phi,T) = \rho_\lambda''(\lambda,\theta,\phi,\theta_r,\phi_r,T) \qquad (3.19)$$

The next reflected quantities to be discussed specify one angle but sum the over the hemisphere for the other. These quantities are directional hemispherical spectral reflectance, and hemispherical directional spectral reflectance. The directional hemisperical spectral reflectance can be defined as the energy reflected into all solid angles divided by the incident energy from one direction. It is also

$$\rho_\lambda'(\lambda,\theta,\phi,T) = \int_{2\pi} \rho_\lambda''(\lambda,\theta_r,\phi_r,\theta,\phi,T)\ \cos\theta_r \delta\omega_r \qquad (3.20)$$

The hemispherical directional spectral reflectance is defined as the reflected intensity in the (θ_r,ϕ_r) direction divided by the integrated average incident intensity. There is one important case where these quantities are interchangeable: when the reflectance of a material irradiated at a given angle of incidence (θ,ϕ) as measured by the energy collected over the entire hemisphere of reflection is equal to the reflectance for uniform irradiation from the hemisphere as measured by collecting the energy at a single angle of reflection (θ_r,ϕ_r) and when (θ_r,ϕ_r) is the same angle as (θ,ϕ) (Siegel and Howell, 1972). This important relation is frequently used in integrating sphere reflectometers. Directional spectral absorptance is equal to one minus directional hemispherical spectral reflectance. It is difficult, however, to build a system that will capture all the reflected energy 2π sterradians. It is possible to build a detector that will detect

the reflected energy in one direction after irradiating the sample with uniform radiation inside a sphere. This is the hemispherical directional spectral reflectance, which can be converted to the directional hemispherical reflectance using the reciprocity relation, and the directional spectral absorptance can then be calculated.

The previous reflectivities have all dealt with spectral radiation. As before, averages taken over wavelength will now be discussed.

Bidirectional total reflectance can be written as

$$\rho''(\theta_r,\phi_r,\theta,\phi,T) = \int_0^\infty \rho_\lambda''(\lambda,\theta_r,\phi_r,\theta,\phi,T)\, L_\lambda{}',_i(\lambda,\theta,\phi)d\lambda \quad (3.21)$$

When the spectral distribution of the incident radiation is the same for all directions or even if

$$L_{\lambda,i}(\lambda,\theta,\phi) = c\, L_{\lambda,i}(\lambda) \quad (3.22)$$

with c an arbitrary constant, then

$$\rho''(\theta_r,\phi_r,\theta,\phi,T) = \rho''(\theta,\phi,\theta_r,T) \quad (3.23)$$

Directional total reflectance has the two obvious cases, directional hemispherical and hemispherical directional. Directional hemispherical total reflectance is the fraction of the total energy incident from one direction and reflected into all directions:

$$\rho'(\theta,\phi,T) = \frac{\int_0^\infty \rho_\lambda'(\lambda,\theta,\phi,T)\ L'_{\lambda,i}(\lambda,\theta,\phi)\delta\lambda}{\int_0^\infty L'_{\lambda,i}(\lambda,\theta,\phi)\ \delta\lambda} \quad . \tag{3.24}$$

Hemispherical directional total reflectance is the fraction of radiation reflected into one direction from radiation incident from all directions. When the incident radiation is uniform over all directions, the hemispherical directional total reflectance is:

$$\rho'(\theta_r,\phi_r,T) = \frac{\int_0^\infty \rho_\lambda'(\lambda,\theta_r,\phi_r,T)\ L'_{\lambda,i}(\lambda,\theta,\phi)\ \delta\lambda}{\int_0^\infty i'_{\lambda,i}(\lambda)\delta\lambda} \quad . \tag{3.25}$$

As in the spectral case, with uniform incident radiation, the two directional total reflectivities are equal:

$$\rho'(\theta,\phi,T) = \rho'(\theta_r,\phi_r,T) \quad . \tag{3.26}$$

Finally, the hemispherical total reflectance is fraction of all the incident energy that is reflected. While it is the result of integrations over wavelength and angle, the order of integration is unimportant.

Interrelationships of Absorptance, Emittance, and Reflectance

Now that all the reflectance quantities have been defined, the relations between them and absorptivity and emissivity can be examined.

For opaque bodies, i.e., no transmission of radiant energy, incident radiant energy is either absorbed or reflected. From this simple relation and Kirchhoff's Law, several further relationships can be written. These are the relationships that make it possible to take a reflectance measurement and obtain an emittance value. These relationships and the conditions under which they apply are important in evaluating the validity of this process.

Consider the case when radiation is incident from a direction (θ,ϕ). For the spectral case, the directional spectral absorptance plus the directional hemispherical spectral reflectance add up to the incident beam:

$$\alpha_\lambda'(\lambda,\theta,\phi,T) + \rho_\lambda'(\lambda,\theta,\phi,T) = 1 \tag{3.27}$$

Kirchhoff's Law can be applied without restriction to yield:

$$\varepsilon_\lambda'(\lambda,\theta,\phi,T) + \rho_\lambda'(\lambda,\theta,\phi,T) = 1 \tag{3.28}$$

For the total case, the quantitites involved are directional total absorptance and directional hemispherical total reflectance:

$$\alpha'(\theta,\phi,T) + \rho'(\theta,\phi,T) = 1 \tag{3.29}$$

Kirchhoff's Law for directional total properties can then be applied under the restrictions that the incident radiation is proportional to a blackbody at the same temperature or the surface is directional gray:

$$\varepsilon'(\theta,\phi,T) + \rho'(\theta,\phi,T) = 1 \quad . \tag{3.30}$$

There are more relationships between absorptivity, emissivity, and reflectance. They are not, however, pertinent to the discussion in the following material.

This chapter covered the basic definitions of emittance, absorptance, and reflectance, some relationships between them, and the conditions under which those relationships are valid. This will enable us to evaluate current measurements techniques, which will be discussed in the next chapter. We will be able to identify errors caused by the fact that some of the assumptions necessary to make these relationships valid may not always be fulfilled. The next chapter will cover the process of taking a reflectance measurement from a common laboratory instrument and deriving a total hemispherical emittance. Based on the material covered in this chapter, it will be shown that a direct emittance measurement must be made, in order to determine accurately the total radiative loss from a particular surface.

CHAPTER 4

EMITTANCE DERIVED FROM REFLECTANCE

Solar photothermal converter performance is often determined more by the total radiative loss than the solar absorptance of the converter. An assessment of converter radiative loss requires knowledge of total hemispherical emittance and the spectral emittance profile over both the solar and infrared region. As explained in Chapter 2, an optimum solar converter material has a spectral profile that is characterized by a step function with high absorptance at wavelengths shorter than 2 microns and low emittance at wavelengths longer than 2 microns. This spectral data is typically obtained from a spectrophotometer used in a reflectance mode. The results of this near normal incidence spectral reflectance (NNISR) measurement can directly show the test material's performance as compared to the optimal spectral profile. This leaves the total hemispherical emittance of the test material at operating temperatures of solar converters to be determined.

The total hemispherical emittance of a material can be obtained by direct measurement. However, since this quantity is related to NNISR through the material's optical constants, n and k, it has become common practice for many groups, including the Solar Energy Group, to use the NNISR data to obtain the total normal emittance. The Fresnel equations can then be modified, if n and k are known, to convert the

total normal emittance into total hemispherical emittance. However, the assumptions needed to derive total hemispherical emittance from a NNISR measurement sometimes cause the result to be only approximate. This chapter will explain the derivation of total hemispherical emittance from a NNISR measurement, and show, using the relationships developed in the last chapter, why the accuracy is limited.

The mode of operation of a typical infrared spectrophotometer must be described to explain how a NNISR measurement is made. Light from a broad-band source is formed into a converging cone and reflected off the sample at an angle near normal, usually 6 to 12 degrees. Usually, the signal derived from this beam is compared to a signal from a similar beam reflected off a reference material, e.g., aluminum. The results are recorded on a strip chart recorder, as a function of wavelength.

The first approximation is made in converting this NNISR into a directional-hemispherical spectral reflectance. The assumption is made that all of our samples are specular, i.e., that all reflection is at angles equal to the angle of incidence. This assumption allows us to equate the NNISR to a directional-hemispherical spectral reflectance. This is equivalent to saying that all the reflected energy in the hemisphere is assumed to be contained in the small solid angle that passes through the detector aperture of the infrared spectrophotometer. No material is perfectly specular; however, some are close. Specularity is both a function of the material and of the smoothness of the surface relative to the wavelength. Our samples were generally thin films

deposited by CVD, which replicates the well-polished surface of the substrate which is smooth at the infrared wavelengths. This assumption will produce some error, the magnitude of which is proportional to the amount of light scattered out of the specular direction, the light reflected but not collected in the detector aperture.

The directional-hemispherical spectral reflectance is easily converted to directional spectral emittance. Assuming the sample is opaque, Equation 3.28 allows us to write

$$\varepsilon_\lambda'(\lambda,\theta,\phi,T) = 1 - \rho_\lambda'(\lambda,\theta,\phi,T) \tag{4.1}$$

Since this is a direct application of Kirchhoff's Law, there are no further restrictions. The assumption of opacity is not unimportant, as it was difficult to make uniform samples big enough to be measured in our equipment, and the opacity was especially important in the infrared here the human eye is inadequate to judge. Fortunately, the infrared spectrophotometer used in a transmission mode did prove the samples to be opaque.

It is relatively easy to obtain a directional total emittance from strip chart record planimetry. Planck's blackbody distribution function enables us to calculate the power radiated by a blackbody in each wavelength interval. So, we integrate over wavelength by summing the products of the blackbody power and the directional spectral emittance in small wavelength intervals, and obtain the directional total emittance.

$$\varepsilon'(\beta,\theta,T) = \frac{\int_0^\infty \varepsilon_\lambda'(\lambda,\beta,\theta,T)Me_\lambda(\lambda,T)\ \delta\lambda}{\sigma T^4} \qquad (4.2)$$

If the assumption is made that emittance is a slowly changing function of temperature, then the integral can be calculated for temperatures different from those at which the NNISR measurement was made. That is emittance can be calculated at converter operating temperatures rather than at room temperatures. Since we know emittance is generally a slowly varying function of temperature, this assumption introduces only slight errors. Unfortunately, most infrared spectrophotometers do not have a large enough spectral range to provide the directional spectral emittance for all the necessary wavelengths. For example, the Solar Energy Group uses a Perkin-Elmer 137 spectrophotometer with a range of 2.5 to 15 microns. However, at 150 C, 25% of a blackbody's energy is contained at wavelengths longer than 15 microns; the necessary long wavelength limit is approximately 30 microns. In this case, a common assumption, with associated error, is that the emittance varies little beyond the last wavelength region measured, so the last value measured is used over the remaining portion of the integral. This is essentially a directional gray assumption at long wavelengths. The alternative is to use blackbody curves for temperatures above 500 C, so that virtually all the radiated energy is in wavelengths below 15 microns. But then, the assumption that the room temperature emittance is the 500 C emittance may break down. These assumptions are not disastrous, but they do make the result slightly inexact. Nevertheless, we now have a total emittance at near normal angle.

Converting the directional total emittance to a hemispherical total emittance requires the use of the Fresnel equations with their associated limitations and assumptions. These assumptions are simply a smooth surface with no contaminants. The Fresnel equations can be used to derive expressions for both the directional total emittance and hemispherical total emittance in terms of n and k. These take into account the function dependence of emittance on direction; for example, the Brewster angle leak, leading to higher emittance, is incorporated into these expressions. The following equations from Siegel and Howell are for normal total emittance

$$\varepsilon_{normal} = \frac{4n}{n^2+k^2+2n+1} \tag{4.3}$$

and hemispherical total emittance.

$$\varepsilon = 4n - 4n^2 \ln\left(\frac{1+2n+n^2+k^2}{n^2+k^2}\right) + \frac{4n(n^2-k^2)}{k}\tan^{-1}\left(\frac{k}{n+n^2+k^2}\right) + \frac{4n}{n^2+k^2} - \frac{4n^2}{(n^2+k^2)^2} \ln(1+2n+n^2+k^2) - \frac{4n(k^2-n^2)}{k(n^2+k^2)^2}\tan^{-1}\left(\frac{k}{1+n}\right) \tag{4.4}$$

Siegel and Howell also state that for long wavelengths, i.e., greater than microns, n and k can be treated as equal. Having done this, they provide a graph showing the ratio of hemispherical total emittance to normal total emittance as a function of normal total emittance. This graph, Figure 4.1, is shown on the following page.

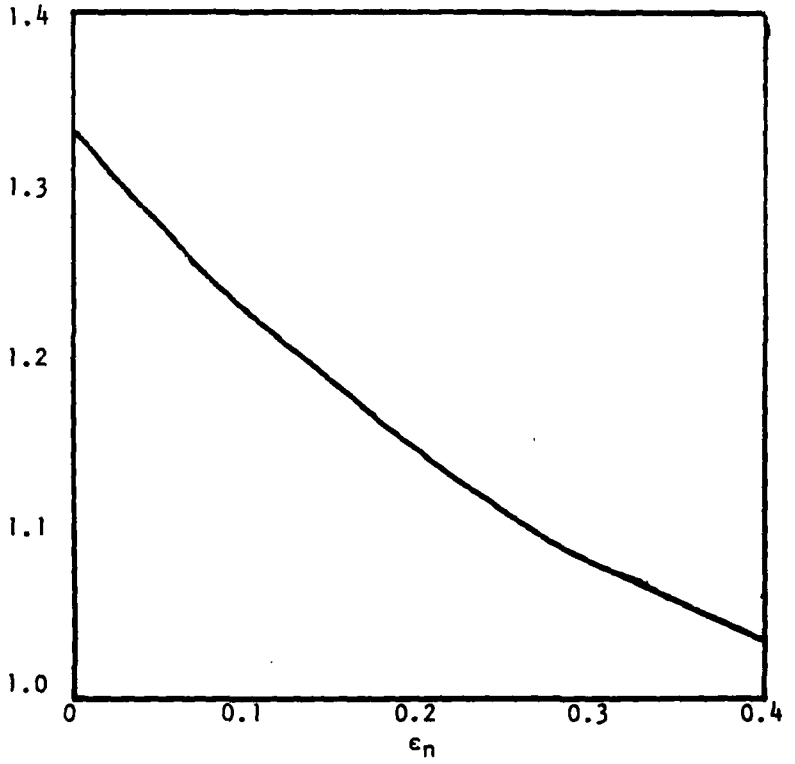

Figure 4.1. Ratio of total hemispherical emittance to total normal emittance as a function of total normal emittance as calculated using the Fresnel equations in the long wavelength limit where n = k (Siegel and Howell, 1972).

There are two problems associated with using the Fresnel equations to convert normal emittance to hemispherical emittance. The equations are based on the assumption of a simple, homogeneous substance, which is certainly not the case for complex materials like "Black Molybdenum". Even using average n and k for the composite compounds may not result in the correct ratio. Also, any sample exposed to air soon builds up a thin oxide layer that acts as an anti-reflection coating with angle and wavelength-dependent properties, also affecting the emittance and causing a deviation from the value derived from the Fresnel equations.

This chapter has shown one way of obtaining total hemisperhical emittance from spectral reflectance. This method assumes a smooth specular opaque directional-gray surface free from any contaminants. It also assumes that the sample's emittance is a slowly varying function of temperature. If not fulfilled, these assumptions introduce error into the derived total hemispherical emittance. Because of the uncertainty associated with this method, a direct means of measuring total hemispherical emittance was needed to gauge the accuracy of this indirect optical method. This method is based on the use of the Calorimetric Vacuum Emissometer (CVE), which will be disucssed in the next chapter. The CVE should allow both the direct measurement of emittance, and for any one group of materials, it should allow the computation of a correction factor to the method described in this chapter, so that the emittance from reflectance derived can be inferred with improved confidence.

Chapter 5

CALORIMETRIC EMISSOMETERS

General Description

The calorimetric measurement of emittance is based on a direct measurement of heat flow into the sample at the equilibrium temperature of the sample. In this method, the sample is thermally isolated from all heat sources except for a measurable power input. This is usually accomplished by suspending the sample in an evacuated chamber by thin wires, which limit the heat loss and yet allow electrical resistive heating. The sample, of course, radiates power according to the Stefan-Boltzmann law; the power radiated by the sample equals the power radiated by a blackbody at the same temperature times the total hemispherical emittance of the sample. The temperature of the sample can be measured by thermocouples or optical means. Because of the thermal isolation, the input power must equal the radiated power. Since the input power is known, and the blackbody radiated power as a function of temperature is obtainable, the emittance can be calculated.

$$\varepsilon = \frac{M}{\sigma T^4} \tag{5.1}$$

The requirement for thermal isolation of the sample can be demonstrated by an assessment of the energy balance of the emissometer. The heat flow into the sample is

$$Q(total) = Q(conv) + Q(cond) + Qsc) + Q(a) + Q(h) - Q(r) \qquad (5.2)$$

where Q(conv) is the heat flow due to air convection, Q(cond) is the heat flow due to heat conduction, Q(sc) is the heat flow from the supports holding the sample, Q(a) is the heat absorbed from other radiating surfaces, Q(h) is the heat flow into the sample from a heat source, and Q(r) is the heat flow out of the sample by radiation. The Stefan-Boltzmann equation can be used to calculate the emittance if all the terms in Eq. 5.2 can be made negligibly small compared to Q(h) and Q(r). Both Q(cond) and Q(conv) become negligible in a high vacuum where there is insufficient air to transport heat energy. Q(sc) is reduced by using narrow wires to limit the heat flow, and even then, a correction factor is usually calculated based on the wires' heat conductivity. Q(a) requires two actions to minimize it. Even at room temperature, the walls of the chamber around the sample are radiating appreciable amounts of energy. The relative effect of this radiation can be reduced to negligible amounts by either heating the sample well above sample temperature or by cooling the walls of the chamber to temperatures well below the sample's temperature. The sample can also absorb reflected energy, radiated by itself and reflected off the chamber walls. The walls, therefore, are usually treated to absorb strongly. This leaves the desired result of a Q(h) that can be accurately measured and a Q(r) so much larger than the other remaining terms that they can be ignored. Further discussion of calorimetric emissometers of this description can be found in a variety of sources (Touloukian and DeWitt, 1970).

The system described in the preceeding section had one drawback for our purposes. The proposed samples were thin films deposited on one side of a substrate, and so the radiative section had to be confined to that one side. This required modifying the usual emissometer. Instead of suspending the sample with wires, the sample was mounted on a block of copper with only the coated side exposed. In between the samples and the block was a thermopile, a collection of themocouples in series on either side of a material of known thermal characteristics, in this case, Kapton™. The thermopile measures heat flow by measuring minute temperature differences between the Kapton surfaces. This not only allowed the direct measurement of the heat flow but eliminated Q(sc) since all heat entering the sample had to enter through the heat flow sensor.

A Detailed Description of the Calorimetric Vacuum Emissometer

The following discussion will cover the actual components of the Calorimetric Vacuum Emissometer, shown in Figure 5.1, and the problems encountered in operating the system. The sample, heat flow sensor, and copper block made up the sample holder. The sample holder was mounted on a large vacuum flange, which contained much of the instrumentation and wiring for the system. The flange was attached to the outer of two chambers, which encloses the sample. The final component of the system was the vacuum system itself.

The sample holder was a 3 x 3 x 3/4 inch copper block. Copper was chosen because its excellent heat conductance would provide uniform

Figure 5.1. Front view of the CVE; from top to bottom, sample chamber, thermocouple selector and readout, ion gauge readout, thermocouple vacuum gauge readout, power supply readout, and power supply.

sample heating. Centered on one of the large faces was a 2 x 2 inch recess milled to a depth of 0.1 inch for the sample. This area held the heat flow sensor, a wafer thin square of Kapton with four thin wires attached at the bottom. A small groove was also milled for these wires. Flush on the surface of the milled area were mounted four thermocouples with their associated wires emerging from the back of the copper block. The sample and heat flow sensor were held in place by four small aluminum clamps screwed down onto the four corners of the sample. Teflon pieces about 1/4 inch square were used to separate and insulate the sample from the aluminum. Four cartridge heaters inserted in the top of the copper block provided the heat source. The copper block itself was mounted on the vacuum flange by two 1/8 inch stainless steel standoffs and a section of 1/4 inch copper tubing. The sample holder in shown in Figure 5.2.

The vacuum flange served as the door to the system and also the interface from the sample to the outer world. The flange contains three sets of vacuum feedthroughs for wires of the thermocouples, thermopile, and the heaters, all of which can be seen in Figure 5.3. The flange also supported parts for two thermocouple vacuum gauges and a port for an ion vacuum guage. The air admittance valve, necessary to return the system to atmospheric pressure, was also mounted here. Twelve bolts and a 12 inch diameter, 1/4 inch thick O-ring provided the necessary vacuum seal for the outer chamber.

Figure 5.2. CVE sample holder with sample.

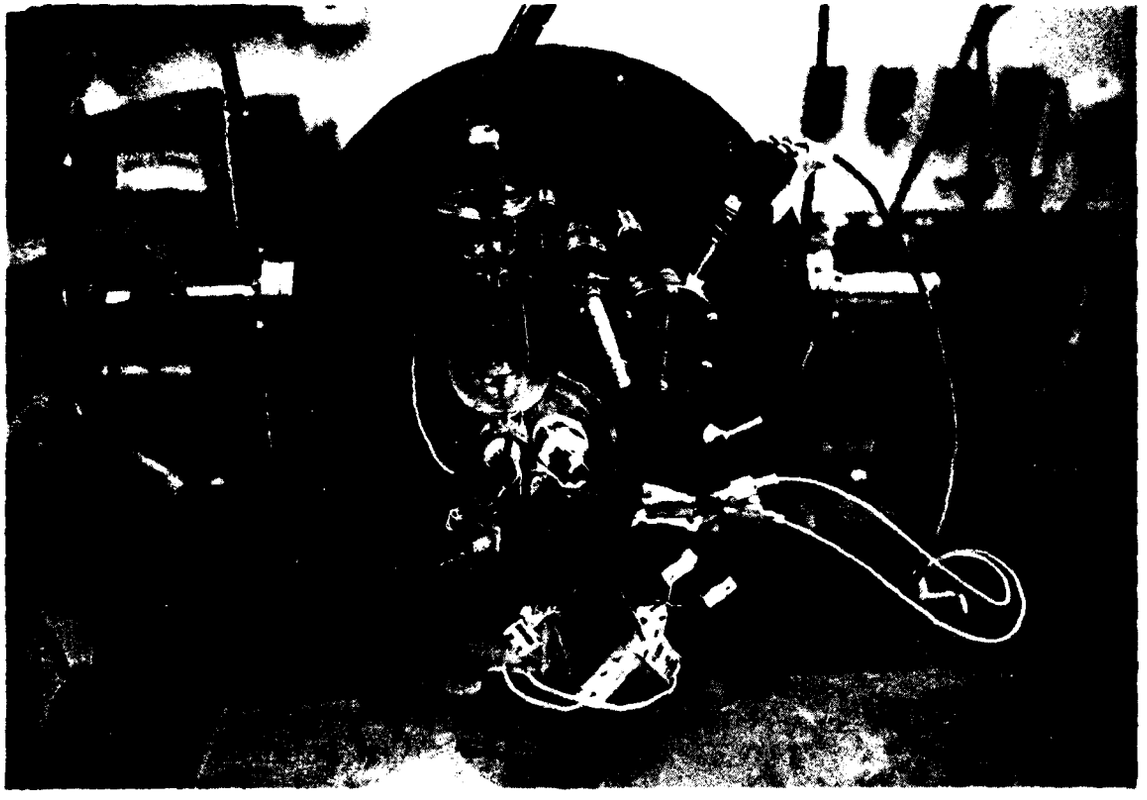

Figure 5.3. Exterior of the vacuum flange of the CVE.

The sample is held inside a double enclosure, an outer stainless steel cylinder and the inner sample cavity. The steel cylinder is approximately 24 inches long and ten inches in diameter. It is mounted horizontally and connects to the diffusion pump underneath through a high vacuum valuve. One end of the cylinder is closed off while the other end has a flange welded to it to mate with the flange previously described. On either side of the flange and of the cylinder are two ports, through which liquid nitrogen is pumped into the sample cavity.

The sample cavity is made of 1/4 inch copper tubing wound and soldered together into a cylinder 6 inches in diameter and 16 inches long. Both ends of the cylinder are capped by 1/8 inch thick copper plates soldered in place. In one end, a square opening was cut in the plate just large enough to accommodate the sample holder without actually touching a side, see Figure 5.4. The two ends of the copper tubing exit the steel cylinder through the two side ports. Liquid nitrogen pumped through the tubing cools the cavity to 77 K, cold enough to eliminate virtually all thermal radiation from the cavity walls. The interior of the cavity has been painted with 3M's Nextel Black Velvet Coating.™ This paint has a measured absorptance of 95%, which reduces the reflected thermal radiation of the sample to a negligible amount. The sample cavity is supported only by the two connections at the liquid nitrogen ports and by a small acrylic spacer which limits heat flow to the sample cavity, diffusion vacuum pump, two valves, three thermocouple vacuum gauges, and one ion vacuum gauge. The mechanical pump is connected by the first valve to either the

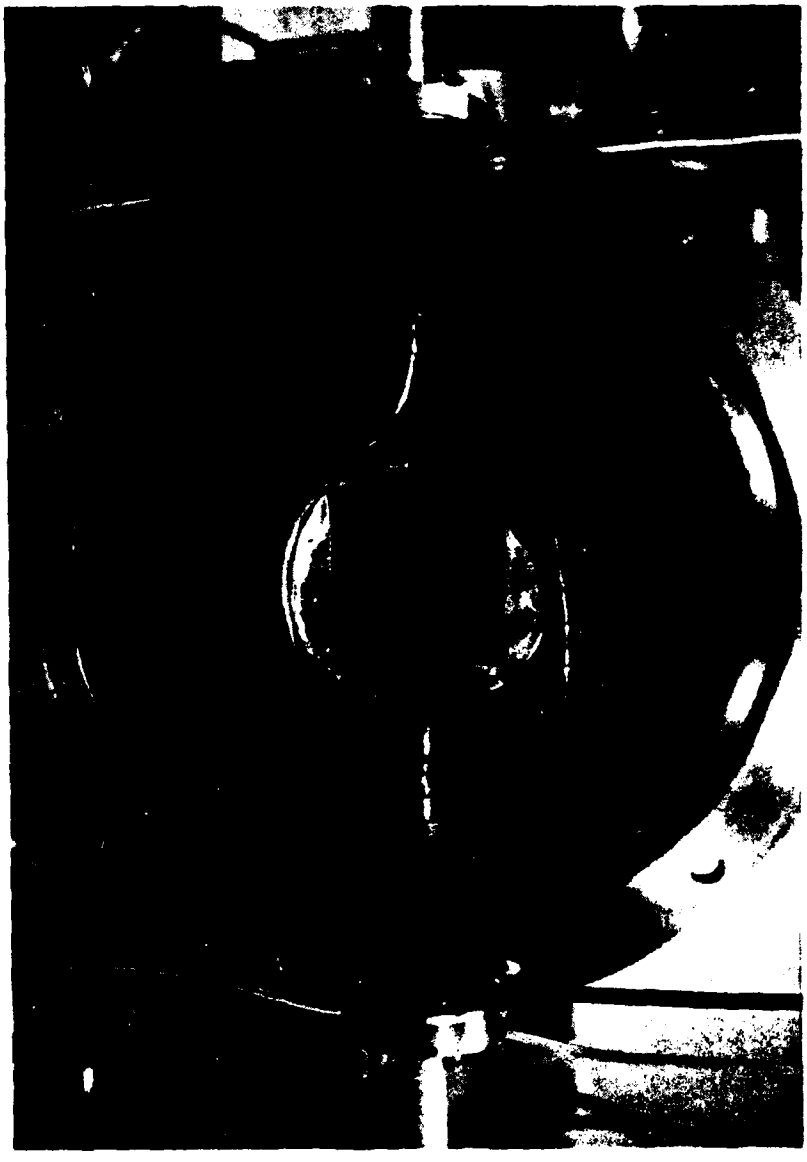

Figure 5.4. Interior of CVE cavity, with cylinder of copper tubing and vacuum ports for liquid nitrogen.

sample chamber or the backing side of the diffusion pump. Initially, the mechanical pump is used to evacuate the sample chamber. Then the mechanical pump is connected to the diffusion pump and through the high vacuum valve, the diffusion pump evacuates the sample chamber to high vacuum. The thermocouple gauges monitor the performance of the mechanical pump in different locations while the ion gauge measures the high vacuum developed by the diffusion pump.

Vacuum problems were the major difficulties encountered on this project. Vacuum problems were finally resolved into two categories, actual leaks and outgassing. Leaks were found in virtually every joint. An attempt to provide rapid cooling of the sample by a cooling water line was abandoned because of the inability to overcome vacuum problems. Another major problem was the interface between the sample cavity tubing and the vacuum ports of the steel cylinder. O-rings were used to provide a vacuum seal but under the thermal stress of cycling from room to liquid nitrogen temperatures, the O-rings soon disintegrated. The O-rings were finally eliminated by making a direct soldered connection, but even this leaked under high vacuum when cooled.

Despite meticulous care in tracking down possible leak sources, the obtainable vacuum was not sufficient to suppress heat loss. Outgassing was then considered. The diffusion pump was left on continuously for several weeks to allow it to clean itself and a small improvement was noted. All unnecessary items were removed from the cavity and the remaining items were cleaned with acetone. This did not help. Finally, the inner painted surface of the sample cavity was targeted as the

culprit. Before cooling by liquid nitrogen, hot tap water was run overnight through the tubing. The temperature of the water was approximately 60 C. The vacuum improved by two orders of magnitude. Unfortunately, every time the sample was changed, the paint re-adsorbed enough gas to require degassing by hot water. This made the emittance measurement a two-day process, one to outgass and prepare the system, and a second for the actual measurement.

Another problem encountered only twice was the formation of a film of foreign matter on the sample surface. This was due to an accidental interruption of the cooling water for the diffusion pump, causing the diffusion pump oil to overheat and contaminate the sample. Fortunately, this was discovered during the initial calibration runs. Afterwards, the samples were measured before and after the emissometer runs in an intergrating sphere reflectometer and the Perkin-Elmer 137 infrared reflectometer to reveal any surface changes. No changes were noted after this procedure was instituted.

The electronics were another source of problems. The basis of the emissometer was the heat flow sensor, a set of thermocouples. Its microvolt output was difficult to measure and several instruments were tried before one was found with enough sensitivity and stability. Chromel-alumel type thermocouples were employed to measure the sample's temperature and were read by an Omega Engineering 199 digital thermometer readout. The thermocouple feedthrough were another major leak source and the wires themselves had to be protected from the heat source, as was found when some shorted after their insulation melted. Several

ion vacuum tubes developed defects or vacuum leaks and had to be replaced.

The final major problem faced was the power source for the cartridge heaters. First, a simple AC power supply was used but was discarded because it was thought to have insufficient power. Next, a commercial temperature controller was used. The temperature controller was a power supply with a thermocouple feedback and logic circuits to maintain the set temperature. This also appeared to have insufficient power until it was found that the copper sample holder was in contact with the sample cavity, a massive heat sink. Once the contact was eliminated, the power problem vanished but another problem appeared. The temperature controller oscillated continuously, and even though the osciallations could be damped, they were apparent on a large scale several hours after starting a run. Since thermal equilibrium was required, the temperature controller was inadequate. The original power supply was returned to the system, and with the thermal contact eliminated, it too had enough power. Although it took 2 to 3 hours to reach thermal equilibrium, this power supply allowed the sample to approach thermal equilibrium in a much more predictable fashion.

The CVE has been described in a qualitative manner in this chapter. The steps taken to reduce unwanted heat flow were detailed. Based on these steps, we have claimed that Equation 5.1 is reduced to Equation 5.2, which allows us to compute emittance directly. A more thorough explanation of the CVE operating procedures is contained in Applendix A. In Chapter 5, Eq. 5.1 is evaluated in a quantitative manner to determine the accuracy of the CVE.

CHAPTER 6

CALIBRATION OF THE CALORIMETRIC VACUUM EMISSOMETER

This chapter is divided into two parts. First, the heat loss balance described by Equation 5.1 is examined in close detail, both for the emittance calculation and for appropriate error limits. Second, to calibrate our instrument against the results of others, two sets of measurements will be compared with values published in the "Thermophysical Properties of Matter, Volume 7, Thermal Radiative Properties", 1970, edited by Touloukian and DeWitt. This comparison will show that our values compare favorably with measurements made by others.

Calculation of Emittance and Relative Error

Equation 5.1 is the basis of this section, and so is repeated here.

$$Q(total) = Q(conv) + Q(cond) + Q(sc) + Q(a) + Q(h) - Q(r) \quad 5.1)$$

Under thermal equilibrium, Q(total) is zero. We have previously implied that first four terms on the right are also zero, so that Q(h), the conductive heat flow into the sample equals Q(r), the heat energy radiated from the sample. We will now examine the magnitude of each term on the right side of Equation 5.1.

The conductive heat flow can be broken into two parts. At higher pressures, heat can be transported by both air conduction and

convection. However, at the operating pressures of the CVE, the distinction is difficult. We will separate them anyway, simply to distinguish between two possible heat transport mechanisms.

Q(conv) is described here as the thermal energy transfer between two surfaces by molecules striking one surface and gaining thermal energy, then colliding with more molecules, with the energy being transferred in each collision until the thermal energy from the first surface finally arrives at the second surface. It is the multiple collisions of air molecules that differentiates this form of heat transfer from conduction. If the pressure is too low to give multiple collisions a finite probability over the dimension of the system, Q(conv) is effectively zero.

A molecule's mean free path is the statistical average distance it travels between collisions. When the mean free path is significantly larger than any interior dimension of the chamber, it is obvious that molecules are traveling directly from surface to surface with no intervening collisions. Kittel, in his book, "Thermal Physics" (1969), defines mean free path as

$$\ell = \frac{1}{\pi d^2 n} \qquad (6.1)$$

where d is the molecular radius and n is the Loschmidt number 2.69 x 10^19 atoms per cubic centimeter at 760 mm of mercury and 0 C. Assuming 5 x 10^ -6 Torr, the mean free path is approximately 5 meters. Since the largest interior dimension is approximately 0.5 meters, it is obvious that few collisions are occurring. It follows that the heat

transfer, Q(conv), based on multiple collisions, is effectively zero (Kittel, 1969).

Q(cond) is the heat transfer by molecule carrying thermal energy directly from surface-to-surface without multiple collisions. The energy transfer per molecule is

$$1/2\ K\ [T(hot) - T(cold)] \qquad (6.2)$$

where the quantity in parentheses is the temperature differential between the hot and cold surfaces and K is the Boltzmann constant. To obtain the total heat flow, the number of molecules striking the sample per second must be obtained. This can be computed from the pressure.

Pressure can be defined as the momentum change per molecule times the number of collisions per unit time per unit area. We will again use 5 x 10^{-6} Torr and so only need to compute the momentum change per molecule to obtain the required number of collisions per unit time per unit area.

The momentum change of a molecule hitting a wall and rebounding in an elastic collision is simply twice the momentum of the molecule in the direction normal to the surface. Since the atmosphere is basically 80% nitrogen and 20% oxygen, we assume that an average molecule's mass is that of air, is 28.8 atomic mass units. The molecule's velocity component perpendicular to the suface can be obtained by the following equation, again from Kittel.

$$\text{average molecular velocity} = \left(\frac{2KT}{\pi m}\right)^{\frac{1}{2}}$$

where K is the Boltzmann constant, T the temperature, and M the mass. With the mass and velocity now computed, the momentum change is also known, and the average number of collisions per unit time per unit area can be calculated. One atmosphere of pressure is 1.013×10^{-6} dynes per square centimeter, which when scaled for our vacuum and then divided by the average momentum change per molecule gives the number of collisions per unit area per unit time. For the temperatures between 50 C to 150 C, the numbers are 2.86×10^{-15} to 2.50×10^{-15} collisions per second per square centimeter. These numbers times the energy transfer per molecule, Equation 6.2, provide the total Q(cond), 1.25 to 1.54×10^{-4} Watts for 50 C to 160 C. These values of Q(cond), when compared to a material with the extremely low emittance of 1% provide a relative error of less than 1%, which will be shown to be much less than our measurable accuracy. Therefore, Q(cond) is effectively zero.

Q(sc) is the thermal energy transfer due to conduction of the supports. Since all the thermal energy entering the sample goes through the heat flow sensor, this is assumed to be neglible. There may be a small unmeasured heat flow through the Teflon spacers and clamps, but since Teflon is an excellent thermal insulator, it is assumed to be unimportant.

Q(a) is the radiant thermal energy absorbed by the sample in the CVE. This term actually consists of two parts, thermal radiation from the walls and the sample's own radiation reflected from the walls. The thermal radiation arriving at the sample from the walls of the cavity is

$$Q(a\text{-rad}) = \sigma T^4 F_{w \to s} A_w \qquad (6.4)$$

where σ is the Stefan-Boltzmann constant, T the temperature of the walls, $F_{w \to s}$ the shape factor that accounts for the geometry and the emittance of the surfaces involved, and Q_w the area of the walls. The product of the sahpe factor and the area is equal to the product of the sample's shape factor and its area, i.e.,

$$F_{w \to s} A_w = F_{s \to w} A_s \tag{6.5}$$

The sample's shape factor can be found in several books on thermal radiation; the one we use was published in an ANSI-ASTM article

$$F_{s \to w} = \frac{1}{1/\varepsilon_1 + A_1/A_2\ (\varepsilon_2 - 1)} \tag{6.6}$$

where ε_1 is the emittance of the sample, A_1, the sample area, ε_2, the walls emittance, and A_2, the area of the walls. The ratio of the areas A_1/A_2 is 0.01 and the emittance of the walls, painted with Nextel Black Velvet , is 0.95 (measured on the Perkin-Elmer 137). Thus, the shape factor is simply the emittance of the sample. Q(a-rad) is then merely the ratio of the wall temperature to the sample temperature, all to the fourth power. To minimize Q(a-rad), the walls are cooled with liquid nitrogen to 77 K. Even at the lowest sample temperature of 50 C, 323 K, the error is only 0.3%.

Q(a-refl) is the thermal energy radiated by the sample and reflected by the walls back to the sample. Since the walls are coated with the highly absorbant paint, only a single reflection need be considered; with each reflection, only 5% of the beam's energy remains. The walls' painted surfaces are very rough, and so radiation incident at angles far from normal gets trapped. Normally incident radiation

that is reflected off the back surface is also reflected into a projected solid angle of π steradians, and the amount in the small solid angle that does return to the sample is so small that it can be neglected.

The remaining terms of Equation 5.1 are the ones to be determined. Q(h) is the heat flow leaving the surface of the thermopile. It is measured by the thermopile, which has an output in microvolts. A simple calculation transforms the voltage into radiated power. This heat flow first crosses a thin coating of vacuum grease and then enters the sample. We assume the thermal resistance across the vacuum grease to be negligible, so that all the power leaving the thermopile enters the sample. The power entering the sample must equal the power being radiated by the sample, Q(r), which is given by the Stefan-Boltzmann Law,

$$Q(n) = Q(e) = \varepsilon\sigma T^4 \tag{6.7}$$

Equation 5.1 has now been completely quantified. Based on the discussion in this chapter, the total hemispherical emittance as determined by the CVE is

$$\varepsilon = \frac{CVA + 1.25\times10^{-4}\,(323/T)^{\frac{1}{2}}\,(T-77)/246}{A\sigma(T^4 - 77^4)} \tag{6.8}$$

where C is the microvolt-watts conversion factor of the thermopile, V is the voltage, A is the area of the sample, 25.8 sq. cm., T is the temperature, and σ is the Stefan-Boltzmann constant. Note that the emittance is a function of temperature and voltage. Although two

factors in this equation have been determined to be negligible, they have been included to ensure that the error calculation is accurate.

The relative error of the emittance measurement is the total differential of emittance divided by the emittance. The total differential of the emittance is

$$|\delta\varepsilon| = \frac{\{CA\delta V + (\tfrac{1}{2}\cdot 1.25\times10^{-4}\ (323/T^3)^{\frac{1}{2}}(T-77)/246}{A^2\sigma^2\ (T^4 - 77^4)^2}$$

$$+ \frac{125\times10^{-4}\ (323/T)/246)\}\delta T}{A^2\sigma^2\ (T^4 - 77^4)^2} \qquad (6.9)$$

$$+ \frac{\{CVA + 1.25 \times 10^{-4}\ (323)/T)(T-77)/246\}\ 4A\sigma T^3\ \delta T}{A^2\sigma^2\ (T^4 - 77^4)^2}$$

Equations 6.8 and 6.9 were the equations used in the determining the emittance and the relative error in all measurements. The relative error varied inversely with the emittance, with emittance values from 0.02 to 0.38 the relative error varied from 11% to 2.8%. This magnitude of error is comparable to other published values. For example, the error limits reported in the "Thermophysical Properties of Matter", when given at all, range from 2% to 20% (Touloukian and DeWitt, 1970).

Based on the above analysis, the CVE is at least as accurate as other calorimeters used to measure emittance. This discussion has all been theoretical, however; only the actual performance of the CVE on known test materials would confirm its accuracy. This is the subject of the next section.

CVE Performance Data

The standard for comparison with our CVE results was the data published in the "Thermophysical Properties of Matter, Volume 7, Thermal Radiative Properties". Aluminum and nickel were chosen as test samples because of the ease in obtaining samples and because many data sets were available on these two materials. The results are shown on the following pages in Figure 6.1 and 6.2, and in Table 6.1 and 6.2. The tables are of CVE data and the graphs show placement of CVE data relative to measurements by others.

The aluminum emittances, as determined by the CVE at 50 C, 100 C, and 150 C, appears to run below other measurements, generally, and to have a scattering of values especially at the 50 C temperature. Two explanations of the lower emittance could be that our samples were smoother than others' samples and that our vacuum was better, both of which are substantiated by the description of their measurements. More substantiation will come in the next chapter when a comparison will be made with the Bennett normal reflectance data. The scattering is harder to explain, except that the CVE vacuum is usually one order of magnitude worse by the end of the last measurement of each emittance at the lower temperature. Also, the aluminum samples varied from new to several years old, which also could explain the deviations.

The nickel CVE data was much more consistent. All three nickel samples produced very similar results. Also, the data from the reference cited was also more consistent for nickel than for aluminum. As shown on the nickel graph, the CVE data appears to fall very close to several other measurements.

The results described in this chapter enabled us to state that the CVE produced accurate results in the measurement of total hemispherical emittance. The CVE then qualified as a standard against which the optically derived emittance could be compared. The next chapter will describe the operation of the CVE, though, before the actual comparison of the optical and calorimetric data is presented.

Table 6.1. Total Hemispherical Emittance Data for Aluminum as Determined by the Calorimetric Method (CVE).

Temperature	Sample #1	Sample #2	Sample #3	Mean
50 C	0.0120	0.0129	0.0150	0.0133
100 C	0.0129	0.0124	0.0124	0.0126
150 C	0.0140	0.0136	0.0131	0.0136

Table 6.2. Total Hemispherical Emittance Data for Nickel as Determined by the Calorimetric Method (CVE).

Temperature	Sampel #1	Sample #2	Sample #3	Mean
50 C	0.0586	0.0579	0.0585	0.0583
100 C	0.0668	0.0668	0.0668	0.0668
150 C	0.0810	0.0802	0.0794	0.0802

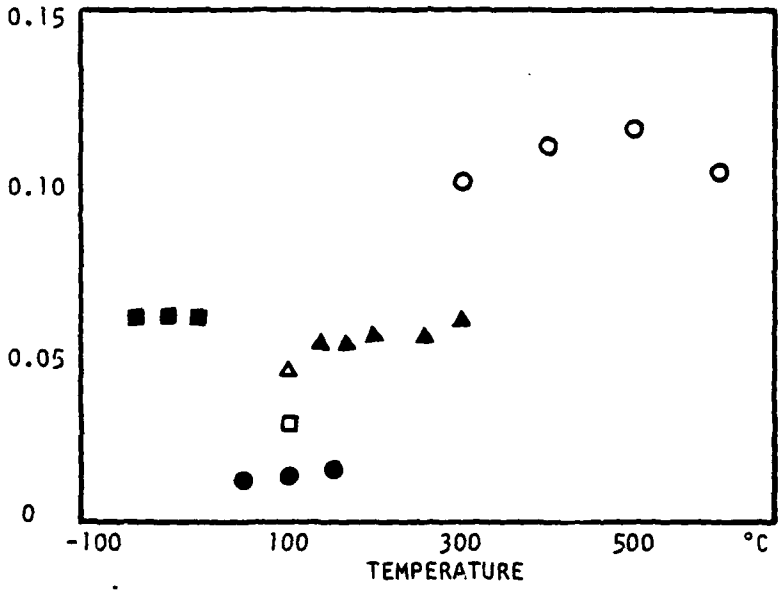

Figure 6.1. Total hemispherical emittance of aluminum as a function of temperature as reported by different measurements.

- ● CVE data
- ○ Calculated from spectral data, #1*
- ■ Plate 0.2 inch thick, hand polished, vacuum 10^{-3} Torr, #31*
- □ 99.99 pure; prefinished with 600 grit aluminum oxide powder on felt, electropolished, vacuum 10^{-5} Torr, #35*
- △ Same as above except bombarded with hydrogen ions (9.840 x 10^{20} ions/cm^2), #38
- ▲ Hollow sphere; polished to approx. 5 microns then rinsed with distilled water and alcohol, dried in nitrogen; measured in vacuum, #40

*Data from Thermophysical Properties of Matter, numbers are data set nos. (Touloukian and DeWitt, 1970).

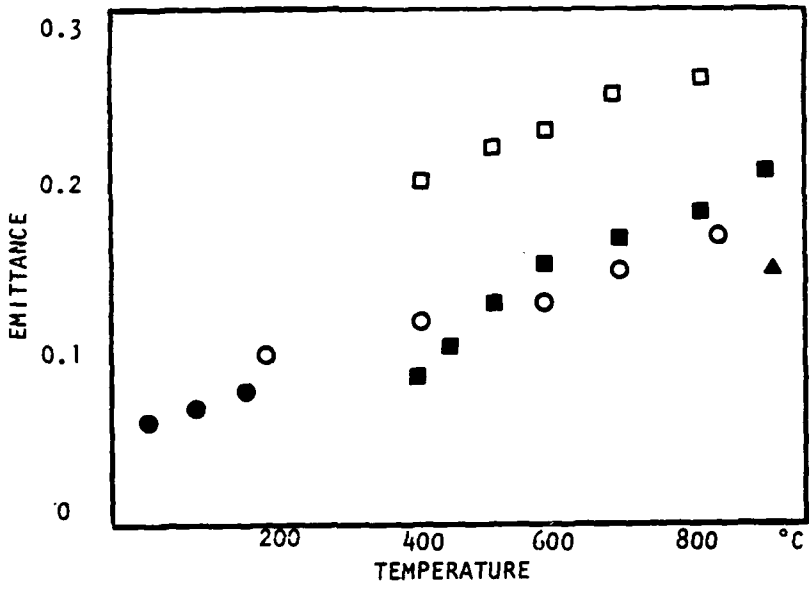

Figure 6.2. Total hemispherical emittance of nickel as a function of temperature as reported by different measurements.

- ● CVE data
- □ Plated on aluminum; buffed; vacuum 10^{-7} Torr, #2*
- ○ Foil 0.0015 in. thick, vacuum 10^{-6} Torr, #3*
- ■ Foil 10^{-5} in. thick, solvent cleaned, 10^{-6} Torr, #10*
- ▲ Foil 0.0005 in. thick, solvent cleaned, 10^{-6} Torr, #11*

*Data from Thermophysical Properties of Matter, numbers are data set nos. (Touloukian and DeWitt, 1970).

CHAPTER 7

RESULTS

This chapter contains the measurements of total hemispherical emittance ε, and total normal emittance ε_n. The ratios of these measured quantities, $\varepsilon/\varepsilon_n$ are also compared with the ratios derived from the Fresnel equations. This data is presented in Tables 7.1 and 7.2. Table 7.3 again presents the ratio, $\varepsilon/\varepsilon_n$, but this time as a ratio of the measured quantity versus the predicted quantity. Table 7.4 shows the relative error in total radiative loss from using NNISR to derive total normal emittance, and then the Fresnel ratio to obtain total hemispherical emittance instead of using the calorimetrically measured total hemispherical emittance. Figures 7.1 through 7.13 show the individual samples total hemispherical emittance and the agreement of the ratio $\varepsilon/\varepsilon_n$ measured with the Fresnel ratio.

Tables 7.1 and 7.2 contain many elements and so will be explained in detail. The two tables separate the measurements made for calibration of the CVE from the actual research done on molybdenum thin films. Under each material is first listed the measured total normal emittance as derived from NNISR. In the case of aluminum, an additional total normal emittance is listed, which was derived from the Bennett data (Bennett, Silver and Ashley, 1963). Following the total normal emittances, in all cases, are the total hemispherical emittances, first as derived from the NNISR and the Fresnel relations, and then,

as determined by the calorimetric method. Then are listed the ratios of total hemispherical emittance to total normal emittance. The first ratio shown is based on the measured quantitites listed above, i.e., the CVE determined total hemispherical emittance and the total normal emittance derived from NNISR measured on the Perkin-Elmer 137. The second ratio is based on the Fresnel expressions. The value listed as the Fresnel ratio was obtained from Figure 4.1, a graph of the ratio as a function of the normal emittance, using the measured total normal emittance as the input.

The four molybdenum samples vary only in annealing time after deposition. The Super Molybdenum sample was annealed at 1000 C for 10 minutes. Samples #1 and #2 were annealed at 700 C for 3 minutes and 1 minute, respectively. Black Molybdenum #3 was as-deposited, i.e., no anneal. The effect of annealing will be discussed in Chapter 8.

Table 7.1. Total Hemispherical Emittance ε, Total Normal Emittance ε_n, and a Comparison of Ratios $\varepsilon/\varepsilon_n$, as Measured and as Predicted Using the Fresnel Equations for Aluminum and Nickel

	Temperature	50 C	100 C	150C
ALUMINUM				
	ε_n	0.020	0.021	0.023
	ε_n (Bennett)			0.019
	ε (Optical)	0.026	0.027	0.030
	ε (Calorimetric)	0.013	0.013	0.014
	RATIO $\varepsilon/\varepsilon_n$			
	CVE/PE137	0.65	0.62	0.61
	FRESNEL	1.30	1.30	1.30
NICKEL				
	ε_n	0.59	0.61	0.61
	ε (Optical)	0.71	0.75	0.74
	ε (Calorimetric)	0.58	0.67	0.80
	RATIO $\varepsilon/\varepsilon_n$			
	CVE/PE137	0.98	1.10	1.31
	FRESNEL	1.23	1.23	1.22

Table 7.2. Total Hemispherical Emittance ε, Total Normal Emittance ε_n, and a Comparison of Ratios $\varepsilon/\varepsilon_n$, as Measured and as Predicted Using the Fresnel Equations for Super Molybdenum, and Black Molybdenum Samples #1, #2, and #3.

Temperature	50 C	100 C	150 C
SUPER MOLYBDENUM			
ε_n	0.020	0.021	0.023
ε (Optical)	0.250	0.026	0.029
ε (Calorimetric)	0.040	0.043	0.050
RATIO			
CVE/PE137	2.00	2.05	2.17
FRESNEL	1.25	1.25	1.24
BLACK MOLYBDENUM #1			
ε_n	0.076	0.072	0.074
ε (Optical)	0.091	0.086	0.088
ε (Calorimetric)	0.103	0.110	0.124
RATIO			
CVE/PE137	1.35	1.48	1.67
FRESNEL	1.20	1.20	1.19
BLACK MOLYBDENUM #2			
ε_n	0.107	0.108	0.111
ε (Optical)	0.125	0.126	0.129
ε (Calorimetric)	0.143	0.149	0.171
RATIO			
CVE/PE137	1.34	1.38	1.54
FRESNEL	1.17	1.17	1.16

Table 7.2. Continued

Temperature	50 C	100 C	150 C
BLACK MOLYBDENUM #3			
ε_n	0.233	0.243	0.273
ε (Optical)	0.251	0.257	0.284
ε (Calorimetric)	0.307	0.345	0.377
RATIO			
CVE/PE137	1.32	1.42	1.38
FRESNEL	1.08	1.06	1.04

Table 7.3. Ratio of Measured to Predicted Ratio of Total Hemispherical Emittance to Total Normal Emittance, Measured by the CVE and Perkin-Elmer 137 Spectrometer and Predicted by the Fresnel Equations.

Temperature	50 C	100 C	105C
ALUMINUM	0.50	0.48	0.47
W/Specular Assumption	0.98	0.98	1.05
NICKEL	0.80	0.89	1.07
SUPER MOLYBDENUM	1.60	1.64	1.75
BLACK MOLYBDENUM #1	1.13	1.23	1.40
BLACK MOLYBDENUM #2	1.14	1.18	1.33
BLACK MOLYBDENUM #3	1.22	1.34	1.33

Table 7.4. Relative Error in Total Radiative Loss from Using Optical Means of Driving Total Hemispherical Emittance as Compared to the Calorimetric Method.

Temperature	50 C	100 C	105 C
ALUMINUM	54%	62%	64%
w/1% Specular Assumption (See Chapter 8)	02%	02%	05%
NICKEL	25%	12%	7%
SUPER MOLYBDENUM	37%	29%	43%
BLACK MOLYBDENUM #1	11%	21%	29%
BLACK MOLYBDENUM #2	12%	15%	25%
BLACK MOLYBDENUM #3	18%	25%	25%

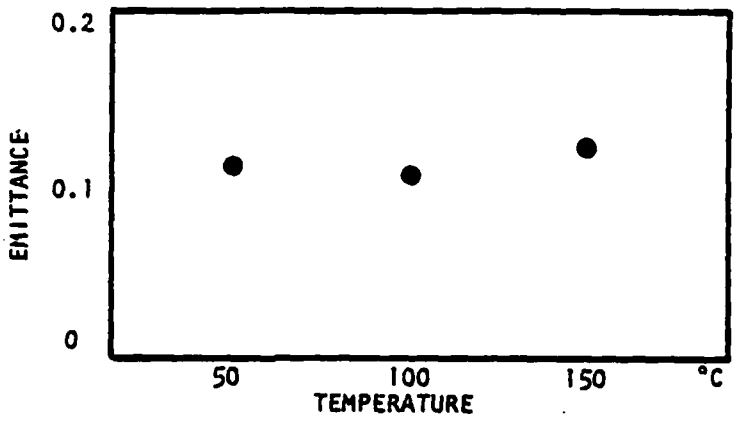

Figure 7.1. Total hemispherical emittance of aluminum as determined by the calorimetric method (CVE).

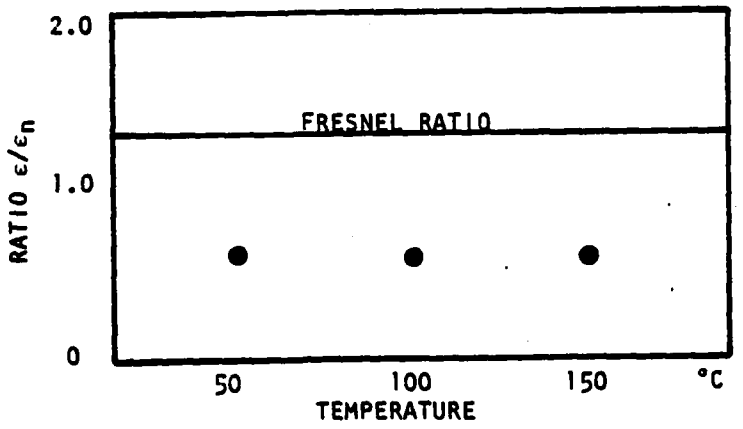

Figure 7.2. Measured and predicted ratios of total hemispherical emittance to total normal emittance for aluminum.

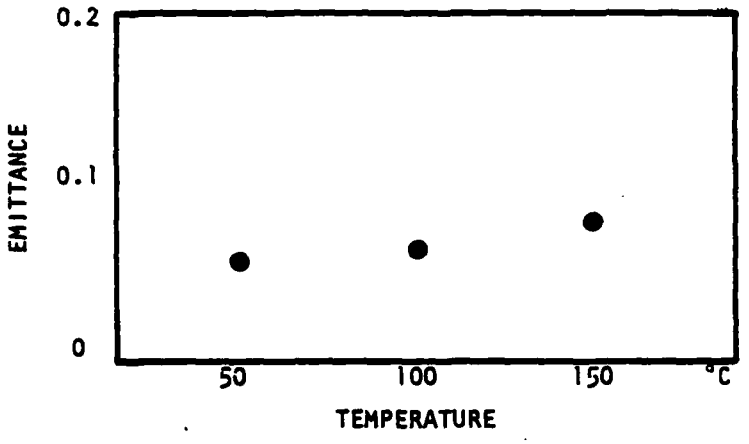

Figure 7.3. Total hemispherical emittance of nickel as determined by the calorimetric method (CVE).

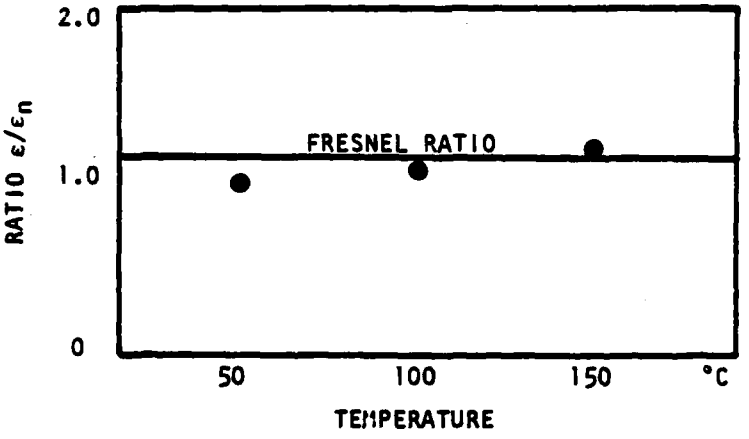

Figure 7.4. Measured and predicted ratios of total hemispherical emittance to total normal emittance for nickel.

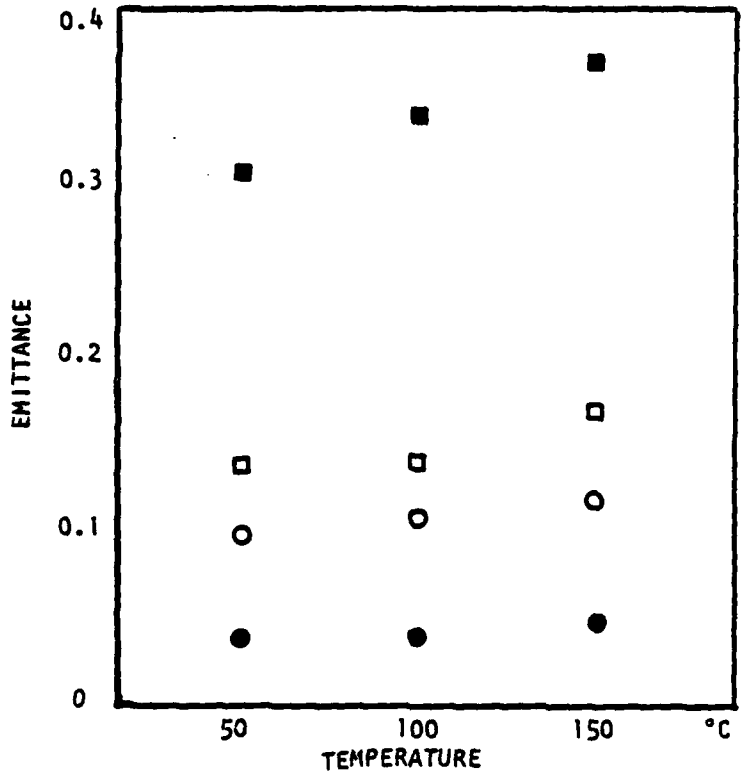

Figure 7.5. Total hemispherical emittance of "Super Molybdenum" and "Black Molybdenum", samples #1, #2, and #3, as determined by the calorimetric method (CVE).

- ● Super Molybdenum
- ○ Black Molybdenum #1
- □ Black Molybdenum #2
- ■ Black Molybdenum #2

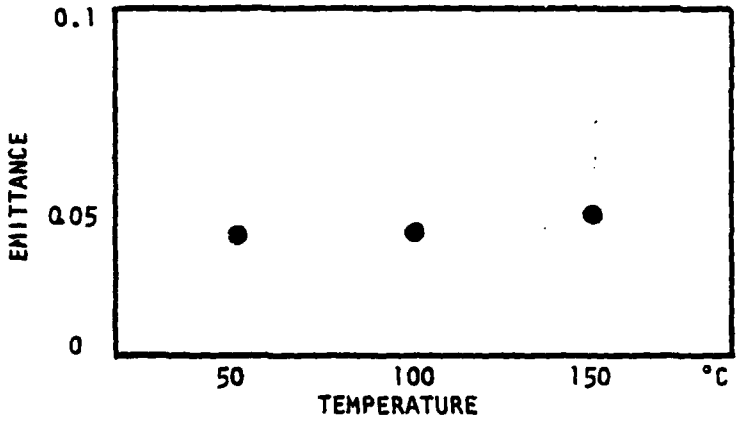

Figure 7.6. Total hemispherical emittance of "Super Molybdenum" as determined by the calorimetric method (CVE).

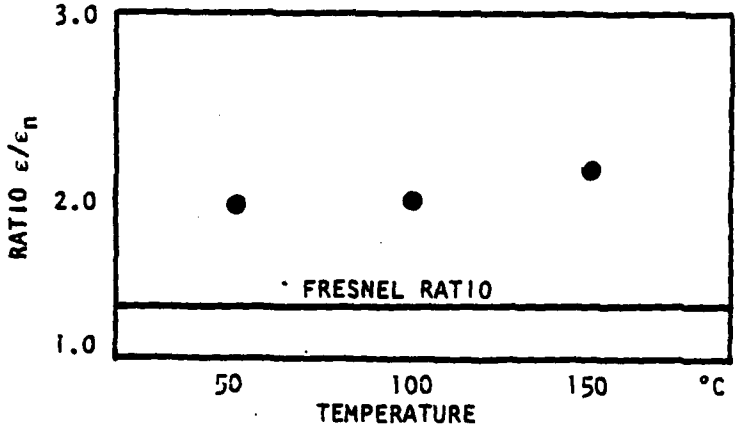

Figure 7.7. Measured and predicted ratios of total hemispherical emittance to total normal emittance for "Super Molybdenum".

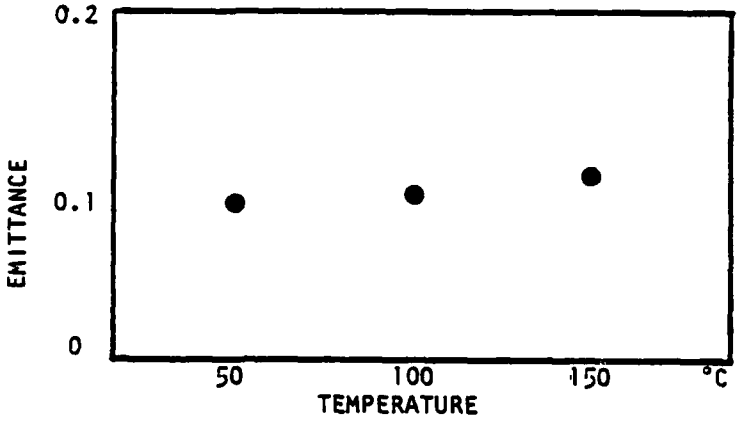

Figure 7.8. Total hemispherical emittance of "Black Molybdenum" #1 as determined by the calorimetric method (CVE).

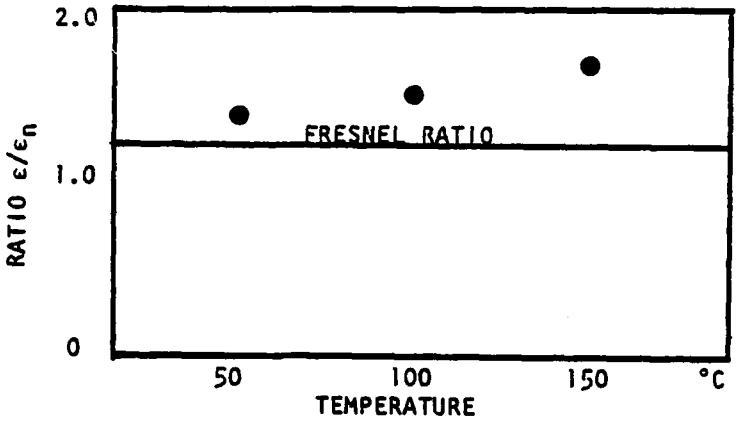

Figure 7.9. Measured and predicted ratios fo total hemispherical emittance to total normal emittance for "Black Molybdenum" #1.

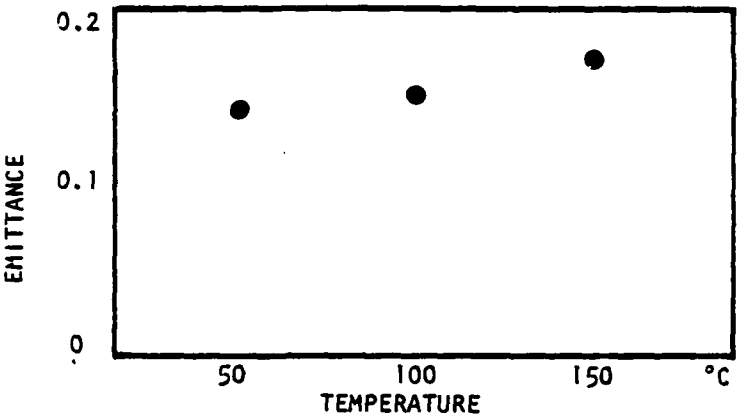

Figure 7.10. Total hemispherical emittance of "Black Molybdenum" #2 as determined by the calorimetric method (CVE).

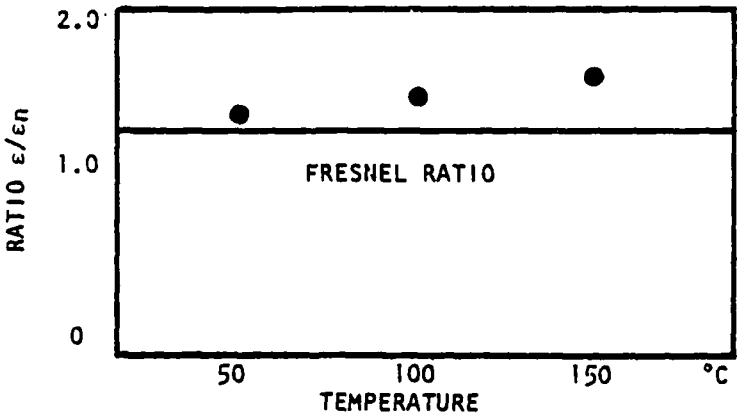

Figure 7.11. Measured and predicted ratios of total hemispherical emittance to total normal emittance for "Black Molybdenum" #2.

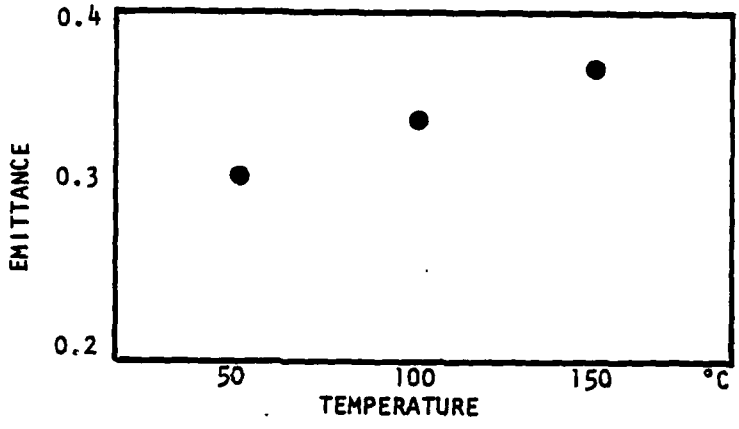

Figure 7.12. Total hemispherical emittance of "Black Molybdenum" #3 as determined by the calorimetric method (CVE).

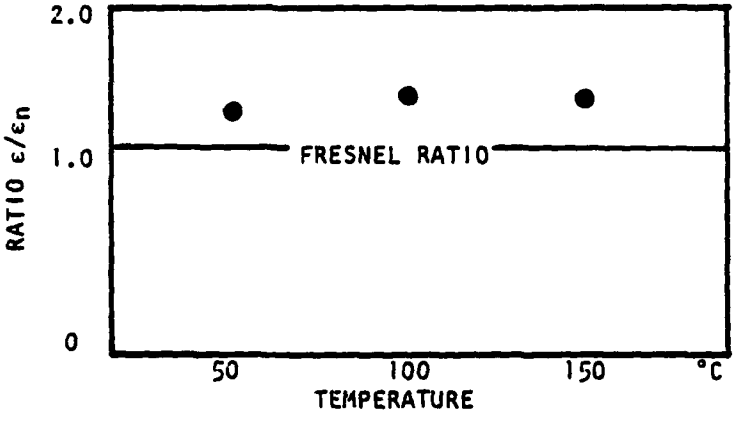

Figure 7.13. Measured and predicted ratios of total hemispherical emittance to total normal emittance for "Black Molybdenum" #3.

CHAPTER 8

DISCUSSION

This chapter deals with the primary purpose of this thesis, a comparison of optical method of determining total hemispherical emittance with the calorimetric method. The calorimetric means was shown in Chapter 6 to be an accurate, direct measurement of the total radiative loss of a material. The optical means of deriving total hemispherical emittance from a NNISR measurement was shown in Chapter 4 to require four assumptions and approximations, which cast doubt on its accuracy. These assumptions and approximations will now be evaluated for their effect on the calculated emittance. This will provide a tool with which the results listed in Chapter 7 can be analyzed.

The first optical measurement assumption is discussed in Chapter 4 was specularity. The optical method is based on a near normal incidence, spectral reflectance measurement. This quantity can be converted to a directional spectral emittance by subtraction from one. We assume the measured quantity is the directional hemispherical spectral reflectance. This is true only if all the reflected radiation is measured by the detector. The detector, however, measures not all the reflected radiation from the surface but only that reflected in a small solid angle around the angle of reflection suggested by geometric ray optics. All the reflected energy would be measured only if the sample

was perfectly specular, but, since there are not perfectly specular materials, the measured reflectance is less than the actual directional hemispherical spectral reflectance and the calculated directional spectral emittance is too large. Thus, the specular assumption leads to an emittance value that is larger than the real emittance.

The second assumption made in the optical determination of total hemispherical emittance assigns to the sample the qualities of a graybody, an assumption required to obtain the directional total emittance from the directional spectral emittance. The directional spectral emittance was calculated from the NNISR measurement, as described in the last paragraph. The directional total emittance is computed by integrating the product of the directional spectral emittance and a blackbody distribution over all wavelengths. The limits of integration can be reduced, however, to those wavelengths for which the blackbody distribution is appreciably non-zero. For a sample at 150 C, these limits are approximately 3 to 30 microns. At 50 C, the long wavelength limit is closer to 40 microns. The directional spectral emittance, calculated from NNISR, only covered the range of 2.5 to 15 microns, due to the limited range of the spectrophotometer. To extrapolate the directional spectral emittance out to the required wavelengths, we assumed that the emittance would vary very little from the value corresponding to 15 microns. This fixed fraction for emittance over the wavelength band is the graybody assumption. The computed directional total emittance would be larger or smaller than the real directional total emittance, depending on whether the real directional spectral

emittance at wavelengths longer than 15 microns was larger or smaller than the 15 micron value. Therefore, the effect of the graybody assumption on the derived total hemispherical emittance can not be determined unless more information on the NNISR or directional spectral emittance is available for wavelengths longer than 15 microns.

The third assumption to be discussed is that emittance is a function slowly varying with temperature. In the last paragraph, the directional total emittance was computed by integrating the product of the directional spectral emittance with a blackbody curve. If emittance varies slowly with temperature, the calculated room temperature directional spectral emittance can be used with blackbody distributions for 50 C, 100 C, and 150 C, with little error. However, it is known that emittance does change with temperature, and generally it increases. This means that at higher temperatures, the calculated directional total emittance is lower than the real directional total emittance.

The last assumption to be discussed is that there are no textural or other surface effects that increase the total hemispherical emittance. The directional total emittance calculated is actually a normal total emittance, which can be converted to a hemispherical total emittance by using the corresponding Fresnel ratio as described in Chapter 4. Surface roughness can increase hemispherical total emittance in two ways. First, surface roughness can increase the actual radiating surface area, allowing more radiation, which appears as an increase in emittance. Second, surface roughness can create small cavities on a surface that radiate like blackbodies with high emittance. The

emittance measured will be the sum of the material's emittance and the high emittance of these cavities, which will be higher than the measured emittance of a smooth sample. Surface oxide layers also generally increase the emittance of materials (Siegel and Howell, 1972). Thus, surface effects can result in a calculated hemispherical total emittance, based on the normal emittance and the Fresnel relations, lower than the real total hemispherical emittance.

We will now summarize these assumptions' effects on the derived hemispherical total emittance before using this information to analyze the results listed in Chapter 7. The specular assumption leads to an emittance value too large. The graybody assumption effect is indeterminate unless more information is available about long wavelength characteristics. The assumption of emittance as a slowly varying function of temperature leads to too low an emittance value at the higher temperatures. And finally, the effect of surface effects is to derive an emittance value that is also too low. All four of these effects can be seen in the data presented.

The first of the data using the above analysis tools is another verification of the accuracy of the CVE. We know that vacuum deposition of aluminum on an optically flat substrate produces a smooth, flat surface. Therefore, we do not expect to see surface effects. The measured total hemispherical emittance of aluminum varies little with temperature, so another possible effect can be discarded. Information is available to analyze the effect of the graybody assumption. The Bennett group has published values of normal spectral reflectance of

aged aluminum out to 30 microns, measured under ultra-high vacuum with a high precision absolute reflectometer. Using this data the normal total emittance of aluminum at 150 C is 0.019 instead of 0.023 as measured by the Perkin-Elmer 137. Nevertheless, our normal total value was reasonably accurate. That our ratio of hemispherical total emittance to normal total emittance is lower than predicted by the Fresnel relations must therefore be the result of specularity. Aluminum is obviously a highly specular material. However, only a one percent non-specularity of aluminum would reduce the normal total emittance to 0.0102. Using this value in the ratio, $\varepsilon/\varepsilon_n$, results in value of 1.27, 1.27, and 1.37, which are close to the Fresnel predicted value of 1.30.

Even if our assumption of one percent non-specularity is wrong, the results show our hemispherical total emittance to be close to the actual value for aluminum. If we ignore specularity, and compute total hemispherical emittance from the Bennett data and the Fresnel ratio, we obtain an upper limit for the hemispherical total emittance of 0.0273, which is below all but the CVE data in Figure 6.1. Again, the conclusion is that the CVE is an accurate emissometer.

The nickel data shows the same effects. The ratios of hemispherical total emittance to normal total emittance are too low for the 50 C and 100 C values, compared to the Fresnel ratio. This is probably due to both the specular assumption and a decreasing emittance beyond 15 microns, just as in the case of aluminum. The higher than predicted ratio for nickel at 150 C is probably due to an actual increase in the emittance from room temperature to 150 C.

The ratios of hemispherical total emittance to normal total emittance for all four molybdenum samples are higher than the Fresnel predictions. The effect of assuming emittance as a slowly changing function of temperature can be seen in all samples except for Black Molybdenum #3. In the other samples, the ratios increased with increasing temperature, just as predicted in the above discussion. The other cause of the ratios being too high, surface effects, can be justified simply by referring to Figure 2.3, a photograph of the surface of Black Molybdenum, which shows the granularity of the surface. The grain sizes range up to approximately micron and their size is a function of the annealing time.

Annealing has two effects on these CVD molybdenum thin films. Before annealing, the thin film is composed largely of molybdenum dioxide. Annealing slowly drives the oxygen out of the film, which drastically reduces its emittance. Annealing also increases the grain size and creates voids, surface effects which result in higher total hemispherical emittance (Carver, 1980). It can be seen that the reduction of oxygen occurs first. The three Black Molybdenum samples all have approximately the same ratio of hemispherical total emittance to normal total emittance, but Black Molybdenum samples #1, #2, and #3, which were annealed for 3, 1, and 0 minutes, have 50 C hemispherical total emittances of 0.103, 0.143, and 0.307. The emittances decrease with longer annealing times. The Super Molybdenum samples have the lowest hemispherical total emittances but the largest ratios of hemispherical total emittance to normal total emittance. This can be

emplained by the annealing out of the thin film the last of the oxygen, which reduces the emittance, and the growth of the molybdenum grains, whose surface effect increases the ratio.

The value of the optical method of deriving hemispherical total emittance from NNISR can now be determined. Table 7.4 shows the relative error in emittance derived by the optical method. Table 7.1 contains values of total hemispherical emittance as derived by the optical method and determined by the calorimetric method. While the errors fluctuate from material to material, the optically derived emittances are, as a class, too low. The optical method could be improved somewhat, however, by the inclusion of additional data. The Optical Sciences Center has a scatterometer which can determine a material's bidirectional reflectance distribution function. This function could serve as an input to the material's specularity, thus eliminating one source of error. This device may also be able to provide a single spectral reflectance measurement at a long wavelength, i.e., 30 to 40 microns, which would help determine the effect of the graybody assumption. The surface smoothness can be determined by scanning electron microscopy, which could determine grain size and provide an input to surface effects. The only assumption left to generate error is that emittance is a slowly varying function of temperature. There simply is no means of quantifying this effect without performing measurements at the desired temperatures. This last assumption will probably be the limiting factor in the accuracy of the optical method of determining total hemispherical emittance.

CHAPTER 9

CONCLUSION

This thesis set out to meet the three goals stated in the first chapter. The importance of total hemispherical emittance to the total radiative loss of a material was stated for space and military applications, and shown for the solar photothermal conversion application. The relations between emittance and the other optical observable functions of n and k were derived. A means of determining total hemispherical emittance from a near normal incidence spectral reflectance measurement was shown and analyzed. A device to measure total hemispherical emittance, the Calorimetric Vacuum Emissometer, was constructed and shown to have a high degree of precision. Measurements were made of the total hemispherical emittance and total normal emittance of aluminum and nickel for calibration purposes, and of several different molybdenum thin films to evaluate their potential for the solar photothermal conversion process. Finally, a comparison of the optical and calorimetric means of determining total hemispherical emittance was made.

The comparison of the two methods of determining total hemispherical emittance was the subject of Chapter 8. The calorimetric method, which gave results with a minimum of assumptions, was used as

the standard against which the optical method was assessed. The optical method required the use of four approximations:

1. sample specularity was required to insure the measured near normal incidence spectral reflectance was all the reflected radiation from the surface.
2. the graybody assumption was used to extrapolate the NNISR to wavelengths beyond the range of the spectrophotometer,
3. the emittance was assumed to be a slowly varying function of temperature so that the optical method could derive emittance at temperature other than at which the NNISR measurement was made, and
4. surface effects were assumed to be neglible so that the Fresnel relations could be used to convert total normal emittance to total hemispherical emittance.

The effect of these assumptions was to introduce error in the derived total hemispherical emittance.

The assumptions listed above did not affect the assessment of the data in the same direction. The specular assumption consistently causes an emittance to be calculated too large. The graybody assumption effect can go in either direction unless additional information is available to characterize the observable quantities at wavelengths longer than the range covered by the spectrophotometer. The effect of assuming emittance to be a function slowly changing with temperature is generally assumed to underestimate the real emittance of the material. Finally, surface effects also result in emittance measurements below

actual values. This last effect dominated throughout the molybdenum thin films.

The results of the above analysis of the optical method of determining total hemispherical emittance suggests that the method be revised. The scatterometer of the Optical Sciences Center can be used to determine the specularity of the sample and to approximate the actual error resulting from the graybody assumption. Electron microscopy and other tests can quantify the surface effects. Only the effect of temperature on emittance cannot be determined without a measurement of the sample at the desired temperature. An improved optical emittance determination, using the above inputs, should result in a more accurate total hemispherical emittance determination from optical measurement.

APPENDIX A

OPERATION OF THE CVE

This appendix is devoted to a detailed description of the operation of the CVE. There are three main subdivisions of the opeation, sample insertion, vacuum system operation and data collection. After some hands-on experience, one person can perform the operation in a two-day cycle without great difficulty.

Sample Insertion

Sample insertion requires opening the CVE, removing an old sample, inserting the new sample in the sample holder, and replacing the vacuum flange on the steel cylinder. The main difficulties are removing and replacing the flange, preferably done by two men, and not contaminating the sample in the process. The main tools for this step are a 9/16 inch open end wrench, a Phillips screwdriver, and a razor blade.

It will be assumed that the sample is prepared on a 3 x 3 inch square substrate. The corners of the sample need to be rounded to fit in the sample holder; quartz substrates can be trimmed by squeezing the vertex of the corner in a pair of pliers until the corner snaps off.

To open the CVE, first isolate the diffusion pump by closing the high vacuum valve. This is the valve that is between the diffusion

pump and the CVE chamber. The handle should be moved counter-clockwise until the overcenter lock is felt to click in place. The mechanical pump should be left backing the diffusion pump. The diffusion pump need not be shut off. The chamber is now isolated and can be brought to atmospheric pressure by opening the valve on the front of the vacuum flange.

Removing the vacuum flange requires a 9/16 open end wrench. Remove the two thermocouple vacuum gauge leads and the ion gauge tube. Then unscrew all but the top two bolds. This is where a second person is helpful. The flange must be supported while the last two bolts are loosened, and it is almost too heavy for one hand, so use caution. The vacuum flange, when removed, can be placed with the sample holder side up on the three armed support built out of 2 x 4's.

A sample in the holder is difficult to extract. Unscrew the four corner clamps, move the aluminum strips to the side and remove the four Teflon™ spacers. It must be done slowly to avoid damaging the thermopile! Use either the screwdriver or the razor blade to pry the edge of the sample out of the depression on the sample holder's face. On the thicker samples, the screwdriver works particularly well in the area where the thermopile leads exit. Once the sample edge is lifted, the thermopile usually needs to be separated from the sample's bottom surface. The danger is bending, and then breaking, the thermopile. The thermopile can be removed safely by sliding the razor blade between the two at a very shallow angle, and slowly lifting up on the thermopile leads. The bottom of the sample will be coated with vacuum grease.

AD-A116 737 AIR FORCE INST OF TECH WRIGHT-PATTERSON AFB OH F/G 20/13
THERMAL RADIATION FROM HOT SURFACES MEASURED BY OPTICAL AND CAL--ETC(U)
1982 G T O'CONNOR
UNCLASSIFIED AFIT/NR-82-3T NL

Use care to avoid getting the grease on the thin film surface as ususally the sample needs to be tested for contamination after the CVE run.

The first step in mounting the new sample is to put on a plastic glove to avoid contamination. Hold the sample only by the edges and be careful. Coat the backside of the sample with vacuum grease; a bead of vacuum grease 1/2 inch long is the maximum amount necessary. Spread it evenly across all the back surface. Lay the sample on the thermopile on the sample holder. Clean the Teflon spacers with acetone and then place them on the four corners of the sample. Position the aluminum corner pieces on top of the Teflon and then gently screw them in place. Pressure may need to be applied to the Teflon spacers to keep them from being squeezed out of position with the final tightening of the screws. Tighten each screw only a little at a time to keep the application of pressure as even as possible.

Reassembling the CVE is simple. Check the large O-ring on the steel cylinder for cleanliness. If necessary, clean with acetone and reapply a thin coat of vacuum grease. With a helper if possible, bolt the vacuum flange back in place, taking care to mount the flange so that the sample holder is aligned with the opening in the sample cavity and with no wires touching the cavity. Tighten all the bolds, then connect the thermocouple vacuum gauge leads and the ion vacuum tube.

Vacuum System Operation

Vacuum system operation is simple but the system needs many hours to reach the proper vacuum. As stated before, the paint used

inside the sample cavity outgasses terribly and this condition needs to be treated before data can be taken.

At this point, the sample is inside the chamber and the vacuum flange is bolted on. Insure that the relief valve on the flange is closed. Switch the mechanical pump from the backing position to the roughing position. In approximately five minutes, the vacuum in the chamber should be better than 50 millitorr. Switch the mechanical pump back to the diffusion pump and then open the high vacuum valve. The thermocouple gauges should be pegged at zero.

To outgas the paint, hot water is run through the sample cavity coils. In the lab, a sink is adjacent to the CVE, and is used for the source and disposal of hot water. The cavity is connected to the faucet by flexible rubber tubing, one end over the faucet and the other over the nearer cavity port. A second rubber hose connects to the cavity port on theother side and then runs over the CVE and into the sink. All connections are clamped for security, as the water is usually circulated overnight. The water pressure should not be high; adjust the pressure so that no, or very little, water leaks out from the base of the faucet. Once the water is turned on, the vacuum in the chamber will become poor. If the ion vacuum gauge is on, it may shut down. In one hour the vacuum improves significantly, and in 6 to 8 hours, the vacuum should be in the 10^{-6} Torr range.

At the same time the hot water is turned on, the power supply to the cartridge heaters should be adjusted to give enough power to heat the sample to approximately 150 C. A setting of approximately 200

milliamps and 80 volts will accomplish this. This will outgas the sample and sample holder at the same time.

Disconnecting the water is simple. Turn off the water and remove only the faucet connection. Place this end in the sink. Take the other hose's free end and connet it to a compressed air source, such as dry nitrogen. Purge the system until virtually all the water is out of the sample coils. At 30-40 psi, this usually takes 3 to 5 minutes. Then disconnect the hoses completely. At this point, the vacuum should be better than 5×10^{-6} Torr.

Data Collection

Data collection is simple but tedious. Liquid nitrogen is run through the sample cavity until the temperature of the sample stabilizes. The temperature is noted along with the input power. From this data the emittance can be measured. For three measurements, at 150 C, 100 C, and 50 C, this process can take from seven to twelve hours. Although the time required depends on the sample, the operator's experience is the main shortcut.

First, the liquid nitrogen must be connected and circulated. Approximately 30 to 40 liters of liquid nitrogen will be used, so check the source accordingly. The dewar of liquid nitrogen is connected by pipe fittings and copper tubing to the cavity port. Caution: The male fitting on the cavity port is soft soldered. When tightening this fitting, use two wrenches, one to hold the male fitting stationary and the other to tighten the fitting. The copper tubing is wrapped with an

insulating material to cut thermal losses. From the other cavity port the tubing enters a small dewar. This was meant to collect the liquid nitrogen for recycling, but this proved too difficult. There is a valve on the fitting into the dewar that can be used to provide backpressure for the system. When the liquid nitrogen is first turned on, this valve should be fully open. When the fitting on the dewar starts to ice over, this valve should be closed until only a little gas escapes. The correct amount will leave the fitting just covered with ice. This slows the rate at which the nitrogen is consumed.

At this point, the sample will start towards an equilibrium temperature, since the power is constant and the environment has reduced all other heat sources. This is a lengthy process but experience can somewhat speed it. The power setting was already mentioned, 200 mA and 80 V. Generally, before the cooling with liquid nitrogen, this will result in a sample temperature above 170 C. For samples of low emittance, the equilibrium temperature will be approximately 150 C. To speed up the process, turn off the power supply and allow the sample to cool down to 160 C, then return the power to the previous setting. By the time the heat flow stabilizes again, the temperature will be close to the equilibrium temperature. Every 15 to 20 minutes check the zero setting of the microvoltmeter, the actual thermopile voltage, and the four sample temperatures. The thermopile reading will stabilize first. The criteria used for equilibrium have been either no change for 45 minutes or readings that fluctuate in temperature both up and down slightly. In the 150 C range, this usually takes approximately 2 hours.

After the 150 C data has been taken, turn off the power supply and allow the sample to cool to approximately 110 C. This will take around 30 minutes. Then turn on the power supply and set it to approximately 150 mA and 60 V. Again take readings every 14 to 20 minutes, and using the same criteria as before, the equilibrium temperature will be reached in about three hours.

For the 50 C data, again turn off the power supply until the sample temperature reaches approximately 60 C, then set the power supply at 125 mA and 40 V. This data point will take three or more hours. The vacuum usually starts to deteriorate at this point. Outgas the ion gauge for 10 to 15 minutes for an accurate reading.

When all three data points are taken, turn off the ion gauge, the liquid nitrogen, and the power supply. It is usually better to leave the sample in the chamber until the next day, to avoid moisture condensing on the cold cavity. Leave the vacuum pumps running.

This appendix has described the operation of the CVE. This information is summarized in a checklist in Figure A-1. Chapter 7 demonstrated that from this data, an accurate emittance can be calculated. The accuracy was shown both in an absolute sense, in that from Equation 5.1 no other terms are large enough to give any significant error, and in a relative sense, comparing CVE measurements with other known, published values.

Table A-1. Checklist for Operation of the CVE.

Sample Insertion

Obtain sample

Close high vacuum valve (directly above diffusion pump, handle moves counterclockwise)

Open air admittance valve (on front oe CVE)

Remove vacuum flange

Remove thermocouple connections and ion gauge

Use 9/16 wrench. CAUTION: flange is heavy

Remove old sample, razor blade or screwdriver. CAUTION: thermopile will stick to bottom of sample, do not damage!!

Mount new sample

Wear rubber gloves

Coat backside of sample with vacuum grease, a bead 1/2 inch long is sufficient, do not get grease on front

Clean Teflon™ spacers with acetone, then screw down corner supports and Teflon spacers on sample

Bolt vacuum flange back on CVE

Replace thermocouple leads and ion gauge

Close air admittance valve

Vacuum System Operation

Switch mechanical pump to roughing (position labeled on valve)

Wait approximately 5 minutes--vacuum > 50 millitorr

Switch mechanical pump to backing (labeled) and open high vacuum valve (clockwise)

Connect rubber tubing to faucet and liquid nitrogen ports on CVE

Table A-1. Continued

Vacuum System Operation (Continued)
Turn on hot water, slightly more than a trickle, no spray from faucet
Turn on power supply--set to approximately 200 mA and 80 V
Wait several hours--overnight. Vacuum $> 10^{-6}$ Torr
Disconnect water tubing from faucet, leave end in sink
Purge system with nitrogen gas until all water out of CVE
Remove all tubing
Data Collection
Connect liquid nitrogen--two large crescent wrenches
Run liquid nitrogen--adjust flow rate with valve on collection dewar
Wait approximately 1 hour, then take readings of temperature, thermopile every 15 minutes until readings are constant for 45 minutes.
Turn off power supply--allow sample to cool to next temperature
Turn on power supply--approximately 160 mA and 60 V
Wait 1 1/2 hours--then take readings as before
Turn off power supply to cool sample to third temperature
Turn on power supply--125 mA and 40 V
Take readings as before
Turn off power supply, ion guage, liquid nitrogen
Wait several hours or overnight to remove sample (reduces condensation on the cold copper tubing)

Table A-1. Continued

Temperature	Voltage	Milliamps
150 C	80	200
100 C	60	160
50 C	40	100

REFERENCES

Annual Book of ASTM Standards, "Standard Test Method for Total Hemispherical Emittance for 20 1400°C", American Soceity for Testing and Materials, Philadelphia, PA (1976).

Bennett, H. E., M. Silver and E. J. Ashley, "Infrared Reflectance of Aluminum Evaporated in Ultra High Vacuum, Journal of the Optical Sciety of America, Vol. 53, No. 9 (Sept 1963), pp. 1089-1095.

Carver, G. E. "Optical Properties of Chemical Vapor Deposited Molybdenum Thin Films". Ph.D. Dissertation, University of Arizona (1980).

Kittel, Charles, Thermal Physics, John Wiley, New York (1969).

Seraphin, B. E., Notes on a series of lectures presented at the 2nd International Symposium on Non-Conventional Energy conducted at the International Centre for Theoretical Physics, Trieste (Italy), (June 1981).

Siegel, R., and J. R. Howell, Thermal Radiation Heat Transfer, McGraw Hill Book Company, New York (1972).

Touloukian, Y. S., and D. P. DeWitt, Thermophysical Properties of Matter, Vol. 7. "Thermal Radiation Properties", Plenum, New York (1970).